IAI
Journals.ASM.org

Protective Role of D-Amino Acid Oxidase against *Staphylococcus aureus* Infection

Hideaki Nakamura,[a,b] Jun Fang,[a,b] and Hiroshi Maeda[b]

Laboratory of Microbiology and Oncology, Faculty of Pharmaceutical Science, Sojo University, Ikeda, Kumamoto, Japan,[a] and Institute for DDS, Sojo University, Ikeda, Kumamoto, Japan[b]

D-Amino acid oxidase (DAO) is a hydrogen peroxide-generating enzyme that uses a D-amino acid as a substrate. We hypothesized that DAO may protect against bacterial infection, because hydrogen peroxide is one of the most important molecules in the antibacterial defense systems in mammals. We show here that DAO suppressed the growth of *Staphylococcus aureus* in a manner that depended on the concentration of DAO and D-amino acid *in vitro*. Addition of catalase abolished the bacteriostatic activity of DAO. Although DAO plus D-Ala showed less bactericidal activity, addition of myeloperoxidase (MPO) greatly enhanced the bactericidal activity of DAO. Furthermore, DAO was able to utilize bacterial lysate, which contains D-Ala derived from peptidoglycan; this could produce hydrogen peroxide with, in the presence of myeloperoxidase, formation of hypochlorous acid. This concerted reaction of DAO and MPO led to the bactericidal action. *In vivo* experiments showed that $DAO^{-/-}$ (mutant) mice were more susceptible to *S. aureus* infection than were $DAO^{+/+}$ (wild-type) mice. These results suggest that DAO, together with myeloperoxidase, may play an important role in antibacterial systems in mammals.

Hydrogen peroxide (H_2O_2), a major reactive oxygen species (ROS), demonstrates bactericidal activity against various microorganisms (14). In mammals, immune cells (macrophages and neutrophils) utilize ROS, such as H_2O_2 and superoxide anion radical, to eliminate infecting bacteria. Furthermore, in the presence of H_2O_2, myeloperoxidase (MPO) oxidizes halide ions (Cl^- and I^-) to produce hypohalous acid (hypochlorous acid [HOCl] and hypoiodous acid). Hypohalous acid is one of the most active ROS and is toxic to various microbes. Neutrophils are major immune cells that utilize HOCl to eliminate infecting bacteria. For neutrophils, a primary source of the H_2O_2 used to generate HOCl is NADPH oxidase (24). H_2O_2 may also have an additional significant role in chronic granulomatous disease, which is a hereditary disease caused by abnormal H_2O_2 production in neutrophils that is primarily due to defective NADPH oxidase (7, 9).

D-Amino acid oxidase (DAO) is another H_2O_2-generating enzyme, which uses flavin adenine dinucleotide (FAD) as a coenzyme. Biochemically, DAO catalyzes oxidative deamination of D-amino acids to yield corresponding α-keto acids, with molecular oxygen (O_2) used as an electron acceptor and, thus, formation of H_2O_2. DAO exists in many organisms, from yeasts to mammals, but not in bacteria. In mammals, DAO is abundant in the kidney, liver, and brain. However, the biological roles of DAO in mammals remain unclear. In the brain, for example, DAO is associated with neurotransmission via modulation of D-serine levels. The enzymatic activity of DAO has been correlated with the incidence of schizophrenia (8).

Moreover, several researchers found DAO in human and porcine neutrophils, which suggests an important antibacterial role for DAO in neutrophils. Robinson et al. reported that DAO is located on the cell surface and DAO is internalized with foreign objects, such as bacteria (26). Reports that purified porcine DAO has antibacterial activity against *Escherichia coli in vitro* and that its activity was enhanced by addition of D-amino acids, as well as by binding of DAO to bacterial cell walls, have appeared in the literature (10, 29).

D-Amino acids (e.g., D-Ala and D-Glu) are integral components of the peptidoglycan of bacterial cell walls and are missing in mammals. We thus hypothesized that DAO may utilize D-Ala generated by target bacteria and that peptidoglycan synthesis may be involved in defense against microbial infections, because D-Ala is ubiquitous in bacteria. DAO activity is also reportedly absent in the kidney in most germ-free mice and is partially restored by injection of D-Ala (21), which suggests that DAO may be induced by cell wall components and thus may protect hosts against bacterial infection. However, some researchers reported no difference in DAO activity in germ-free mice and conventional mice (23).

In this study, we investigated the potential role of DAO as an antibacterial defense enzyme by using a porcine recombinant DAO, as well as *in vitro* and *in vivo* experiments with DAO-deficient mice and *Staphylococcus aureus*. The combined effect of DAO and MPO was also investigated.

MATERIALS AND METHODS

Materials. The *S. aureus* strain ATCC 25923 was used in this study. ddY mice were purchased from Japan SLC, Inc., Shizuoka, Japan. Soybean casein digest (SCD) broth was purchased from Nissui Co., Tokyo, Japan. Leupeptin, phenylmethylsulfonyl fluoride (PMSF), and FAD were purchased from Sigma-Aldrich Chemical Co., St. Louis, MO. 3-[(3-Cholamidopropyl)dimethylammonio]-1-propanesulfonate (CHAPS) and SBT [*N*,*N*′-bis (2,4-disulfobenzyl) toluidine] was purchased from Dojindo Chemical Laboratories, Kumamoto, Japan. TaKaRa Ex *Taq* was purchased from Takara Bio Inc., Shiga, Japan. PflMI restriction enzyme was purchased from New England BioLabs (Ipswich, MA). SCD agar, isopropyl-β-D-thiogalactopyranoside, carbenicillin, polyoxyethylene sorbitan

Received 1 December 2011 Returned for modification 2 December 2011
Accepted 12 January 2012
Published ahead of print 25 January 2012
Editor: S. R. Blanke
Address correspondence to Hiroshi Maeda, hirmaeda@ph.sojo-u.ac.jp.

doi:10.1128/IAI.06214-11

0019-9567/12/$12.00 Infection and Immunity p. 1546–1553

monolaurate (Tween 20), ammonium sulfate, Tris, EDTA, sodium dodecyl sulfate (SDS), proteinase K, casein sodium, and others were purchased from Wako Pure Chemical Industries, Ltd., Osaka, Japan.

Production and purification of recombinant DAO. Recombinant porcine DAO was prepared as described previously (12). Briefly, the *E. coli* BL21(DE3) strain harboring a pET3c plasmid encoding porcine DAO was cultured in LB medium containing 50 μg/ml carbenicillin as usual, and 0.01 mM isopropyl-β-D-thiogalactopyranoside was added to allow expression of DAO in *E. coli*. After culture for 20 h at 37°C, the bacterial pellets were sonicated (150 W; 30 min) in 20 mM pyrophosphate buffer (pH 8.2) at 4°C. DAO was obtained by means of ammonium sulfate precipitation after heat denaturation, followed by DEAE cellulose column chromatography. The purity of the DAO was checked by means of SDS-polyacrylamide gel electrophoresis (PAGE) with Coomassie brilliant blue staining (purity > 90%).

Assay for bacteriostatic and bactericidal activities. (i) Bacteriostatic activity. *S. aureus* was cultured until the mid-log phase of growth in SCD broth with reciprocal shaking at 1.5 Hz and 37°C. Then, the bacteria were washed twice with physiological saline (0.85%), and 1×10^6 CFU/ml of *S. aureus* was incubated with DAO (2 to 40 μg/ml), D-amino acids (D-Ala [1 to 10 mM], D-Pro [0.3 to 10 mM], D-Glu [10 mM], or D-Asp [10 mM]), and catalase (1 mg/ml) in SCD broth at 37°C for 5 h. The optical density at 570 nm was used to compare relative bacterial cell numbers for the different conditions tested.

(ii) Bactericidal activity. *S. aureus* (1×10^6 CFU/ml), which was prepared as described above, was incubated with DAO (10 to 200 μg/ml), D-amino acids in the same concentration range mentioned above, and MPO (3.2 U/ml) in 50 mM phosphate-citrate buffer (pH 5.5), or the bacteria were incubated with DAO (10 to 50 μg/ml) and the above-described D-amino acids in 10 mM phosphate-buffered saline (PBS) (pH 7.4) at 37°C in a shaking (1.5 Hz) water bath for 30 min. Duplicate 100-μl aliquots of each dilution were added to 15 ml of SCD agar and mixed well in petri dishes for colony formation. The numbers of colonies formed were determined after overnight incubation at 37°C.

Measurement of hydrogen peroxide production. Hydrogen peroxide was measured by colorimetric assay using peroxidase-coupled oxidation of *o*-dianisidine. DAO (5 μg/ml), bacterial lysate (0.5 to 1.0 mg/ml), and horseradish peroxidase (6.6 μg/ml) were incubated in 50 mM phosphate buffer (pH 7.4) containing *o*-dianisidine (75 μg/ml) at 25°C, and then absorbance at 460 nm was measured. Bacterial lysate was prepared by acid hydrolysis of *S. aureus*, hydrolysis in 6 M HCl at 110°C for 24 h, and was then kept in a desiccator containing pellets of NaOH under vacuum to remove the HCl and dried to obtain a powder.

Measurement of hypohalous acid generation. The amount of hypohalous acid (HOCl) was measured by a colorimetric method based on SBT. Briefly, an H_2O_2-generating system (200 μg/ml DAO and 10 mM D-Ala), 0.8 or 1.6 U/ml MPO, 200 mM NaCl, and 5 mg/ml potassium iodide were incubated with 0.1 mg/ml SBT in 50 mM phosphate citrate buffer (pH 5.5), after which the absorbance at 675 nm was measured (27). In another experiment, a lysate of *S. aureus* was used instead of D-Ala.

Genotyping. Genomic DNA was extracted from the auricles of ddY mice after incubation of auricular tissue in lysis buffer (10 mM Tris-HCl, 10 mM EDTA, 0.5% SDS, 0.5 mg/ml proteinase K) at 55°C for 6 h, after which the genomic DNA was purified by phenol-chloroform extraction and ethanol precipitation. The mouse *Dao* gene was amplified by means of PCR using 5′-mDAO and 3′-mDAO primers. The PCR products were also subjected to phenol-chloroform extraction and ethanol precipitation, followed by digestion with the restriction enzyme PflMI. The digested DNA fragments were then separated using 1% agarose gel electrophoresis. The primer sequences used for mouse *Dao* genotyping were as follows: 5′-mDAO, ATGTACGAAGCTGGAGGACAGAGGGG, and 3′-mDAO, CAAGCAGACAGGGCAAGCTCTTCATGG.

Quantification of bactericidal activity in kidneys. Six-week-old female ddY mice were injected with 1×10^7 CFU of *S. aureus* via the tail vein. Three days after bacterial challenge, the mice were sacrificed and the kidneys were excised. The kidneys were homogenized in 1% CHAPS in RPMI medium, and the homogenates were serially diluted with physiological saline. Duplicate 100-μl aliquots of each dilution were added to 15 ml of SCD agar at about 45°C and mixed vigorously in petri dishes. The numbers of viable bacteria were assessed by counting the colonies formed on SCD agar plates after overnight incubation at 37°C.

Measurement of DAO enzymatic activity. Kidneys or peritoneal neutrophils were homogenized using a Polytron homogenizer (Kinematica AG, Lucerne, Switzerland) or by ultrasonication (type Dr. Hielscher, UP50H homogenizer, tip drip type) in ice-cold suspension buffer (100 mM Tris-HCl, pH 8.0) containing a mixture of protease inhibitors (1 mM PMSF, 10 μg/ml leupeptin, and 2.5 mM EDTA). The tissue lysates obtained were then centrifuged (12,000 × *g*; 15 min at 4°C), and each supernatant specimen was used for measurement of DAO enzymatic activity. The DAO activity in the tissue lysates was determined on the basis of formation of α-keto acid (pyruvic acid) during the reaction between D-Ala and DAO, as described previously (11).

Preparation of mouse peritoneal neutrophils. Mouse peritoneal neutrophils were elicited by using a peritoneal injection of 3 ml of 6% casein sodium salt dissolved in physiological saline and harvested via peritoneal lavage 6 h later with 5 ml of PBS. Contaminating erythrocytes were removed by causing them to burst in hypotonic saline solution (0.2% NaCl); isotonicity was then restored with a rebalancing solution (1.9% NaCl), followed by centrifugation. Approximately 1×10^7 neutrophils were obtained from 10-week-old female ddY mice. The purity of the neutrophils was evaluated by means of Giemsa staining under a microscope.

Bactericidal activity of mouse neutrophils with wild-type ($DAO^{+/+}$) and DAO-deficient ($DAO^{-/-}$) mice. *S. aureus* bacteria at the mid-log phase in SCD broth as described above were washed twice with physiological saline and suspended in PBS containing 1 mM $MgCl_2$ and 1.5 mM $CaCl_2$, and the bacteria were treated with 10% pooled mouse serum at 37°C for 15 min for endocytosis after opsonization of *S. aureus* with mouse serum. Then, neutrophils were added to the bacteria at a 1:1 ratio of bacteria to neutrophils (4×10^6 cells/ml) in PBS supplemented with 1 mM glucose and 10% mouse serum for opsonization and incubated at 37°C. After 90 min of incubation, each sample was diluted in 0.2% Tween 20 and incubated for 5 min at room temperature to lyse the neutrophils and release phagocytosed bacteria, after which samples were vortexed vigorously and duplicate 100-μl aliquots were plated on 15-ml agar gel plates of SCD medium, followed by overnight culture at 37°C. The viable bacteria were then counted.

RESULTS

***In vitro* bacteriostatic activity of DAO.** We first examined the bacteriostatic activity of DAO against *S. aureus*. *S. aureus* bacteria were incubated with porcine DAO at various concentrations in the presence of 10 mM D-Ala in SCD medium. A concentration of 2 μg/ml DAO showed 50% bacterial growth suppression, and complete growth suppression was observed with DAO at more than 10 μg/ml (Fig. 1a). Similar concentration-dependent bacteriostatic activity was seen with D-Ala in the presence of 10 μg/ml of DAO (Fig. 1b). This bacteriostatic activity of DAO was not observed with the addition of L-Ala (Fig. 1a). Further, addition of 1 mg/ml catalase abolished the bacteriostatic effect of DAO completely (Fig. 1c), which suggests that H_2O_2 is the major effector of DAO-induced bacteriostatic effects. Though addition of D-Glu and D-Asp could not suppress *S. aureus* bacterial growth, D-Pro suppressed the growth of *S. aureus* more extensively than D-Ala in a dose-dependent manner (Fig. 1d and e).

Enhancement of the bactericidal effect of DAO with MPO *in vitro*. We also examined the bactericidal activity of DAO against *S. aureus*. DAO showed only weak bactericidal activity, even in the presence of 5 mM D-Ala; about 40% decreases in viable bacteria were observed (Fig. 2a). Next, we examined the bactericidal activ-

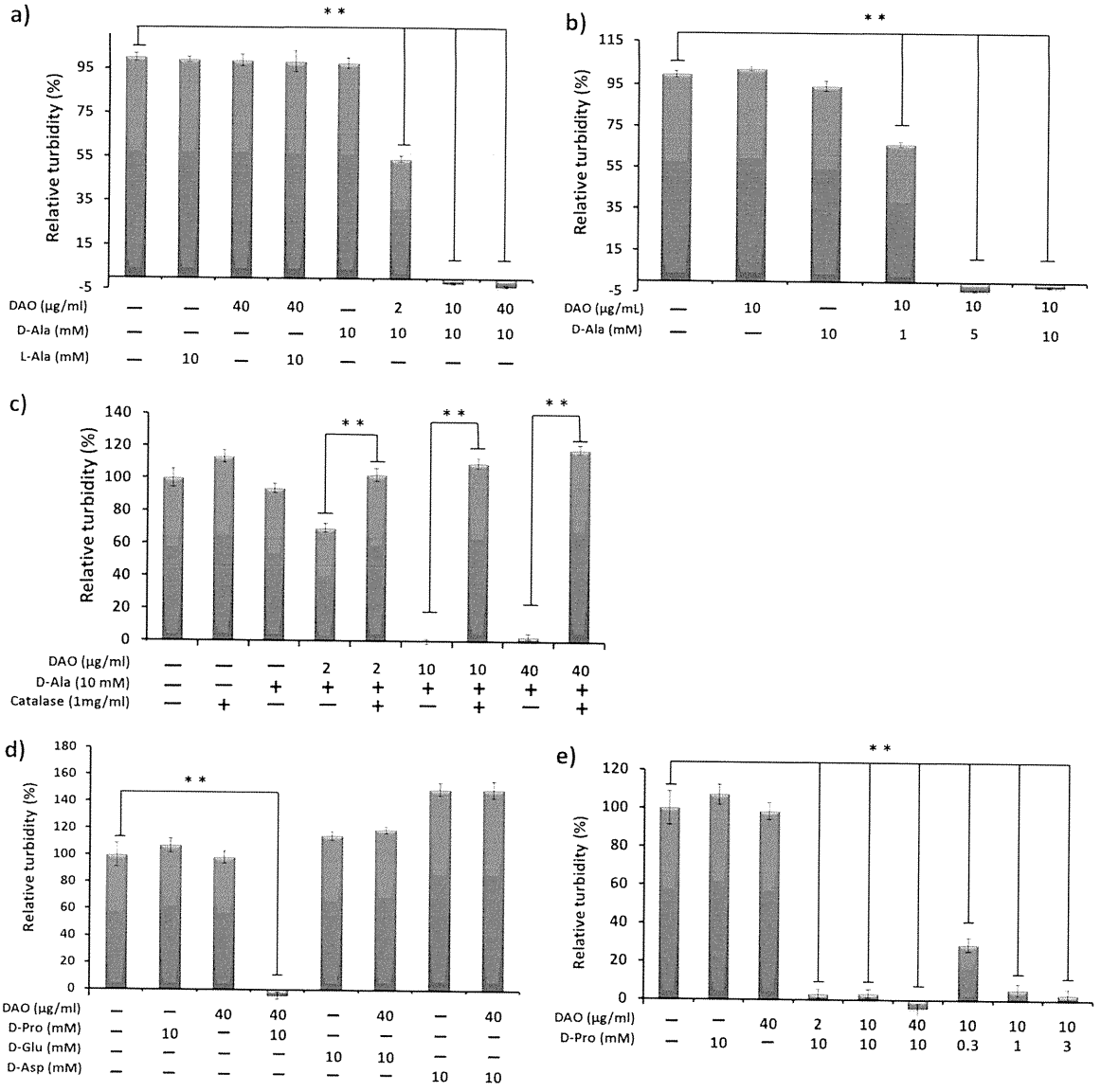

FIG 1 Bacteriostatic activity of DAO against *S. aureus*. (a and b) *S. aureus* (1×10^6 CFU/ml), which was grown until the mid-log phase in SCD broth, was incubated with increasing concentrations of DAO in the presence of 10 mM D-Ala (a) or increasing concentrations of D-Ala in the presence of 10 μg/ml DAO (b) in SCD broth at 37°C for 5 h, and then the optical density at 570 nm was measured. (c) *S. aureus* (1×10^6 CFU/ml) was incubated with DAO and D-Ala, with or without 1 mg/ml (5,000 to 10,000 U/ml) of bovine catalase, and then the optical density at 570 nm was measured. (d and e) *S. aureus* (1×10^6 CFU/ml) was incubated with DAO in the presence of D-amino acids (D-Pro [0.3 to 10 mM], D-Glu [10 mM], or D-Asp [10 mM]) in SCD broth at 37°C for 5 h, and then the optical density at 570 nm was measured. The values are means and standard deviations (SD). **, statistically significant differences ($P < 0.01$) by Student's *t* test.

ity of DAO in relation to that of MPO. Generation of hypohalous acid was detected by means of the SBT-based colorimetric method as described in Materials and Methods (27). Hypohalous acid was generated when the H_2O_2-generating system (DAO and D-Ala) was mixed with MPO and chloride ion (Fig. 2b). These results indicated that DAO serves as an H_2O_2 donor for MPO to generate HOCl.

We next examined the bactericidal activity of the DAO-MPO system. DAO alone showed no bactericidal activity at pH 5.5, but coincubation of DAO and D-Ala showed significant bactericidal activity; about 60% bacterial killing was achieved compared with the control under our experimental conditions (Fig. 2c, lane 7). When three components, DAO, D-Ala, and MPO, were incubated with bacteria, the highest bactericidal activity (more than 99% killing) among the conditions tested was obtained (Fig. 2c, lanes 10 to 14). Similar results were obtained using D-Pro; coincubation of D-Pro, DAO, and MPO showed the highest bactericidal activity against *S. aureus* (Fig. 2e and f); however, this was not the case with D-Glu and D-Asp (Fig. 2d and e).

Use of bacterial D-amino acid by DAO and generation of HOCl in the presence of MPO. Essentially all bacteria produce D-amino acids for the biosynthesis of peptidoglycan, the crucial component of the bacterial cell wall. We investigated whether DAO can use the bacterial lysate, which contains D-amino acids. Use of a D-amino acid, such as D-Ala, for DAO was examined by measuring the production of pyruvic acid, as well as generation of H_2O_2. Acid hydrolysate of *S. aureus* was used as the source of the bacterial D-amino acid. Incubation of the lysate with DAO led to

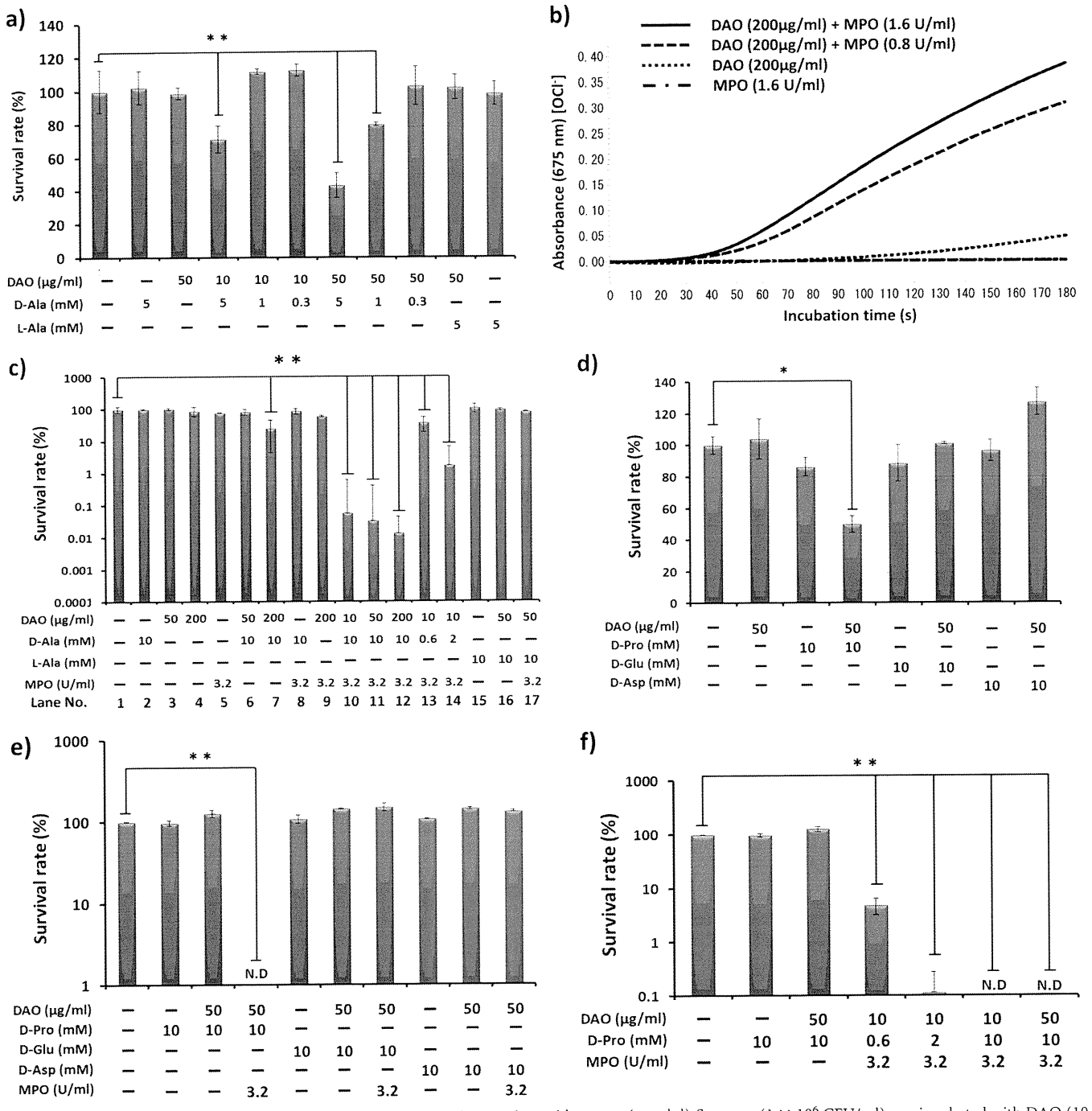

FIG 2 Generation of HOCl and bacterial killing by the DAO–MPO–D-amino acid system. (a and d) *S. aureus* (1×10^6 CFU/ml) was incubated with DAO (10 to 50 μg/ml) and D-amino acid (D-Ala [0.3 to 5 mM], D-Pro [10 mM], D-Glu [10 mM], or D-Asp [10 mM]) in 10 mM phosphate-buffered saline (pH 7.4) at 37°C for 30 min, and then each reaction mixture was diluted in physiological saline, mixed with warm SCD agar, and plated on petri dishes. The bacterial colonies were counted after overnight culture at 37°C. The values are expressed relative to the control. (b) DAO (200 μg/ml) was incubated with or without MPO in 50 mM phosphate citrate buffer (pH 5.5) for the indicated time in the system containing 10 mM D-Ala and 0.1 mg/ml SBT, an indicator of HOCl generation, and absorbance at 675 nm was then measured. (c, e, and f) *S. aureus* (1×10^6 CFU/ml) was incubated with a combination of DAO (10 to 200 μg/ml), D-amino acid (D-Ala [0.6 to 10 mM], D-Pro [0.6 to 10 mM], D-Glu [10 mM], or D-Asp [10 mM]), and MPO (3.2 U/ml) for 30 min in 50 mM phosphate citrate buffer (pH 5.5). The viable bacteria were counted by colony-forming assay as described above. The values are means and SD. N.D., not detected. ** and *, statistically significant differences ($P < 0.01$ and $P < 0.05$, respectively) by Student's *t* test.

significantly increased pyruvic acid production (Fig. 3a). Furthermore, generation of H_2O_2 was measured by incubation of the lysate of *S. aureus* and DAO (Fig. 3b), and HOCl was also generated in the presence of MPO (Fig. 3c). Indeed, coincubation with bacterial lysate, DAO, and MPO produced significant bactericidal activity (Fig. 3d). These results indicate that DAO can utilize bacterial lysates as a source of D-amino acid to generate H_2O_2, which is converted HOCl by MPO.

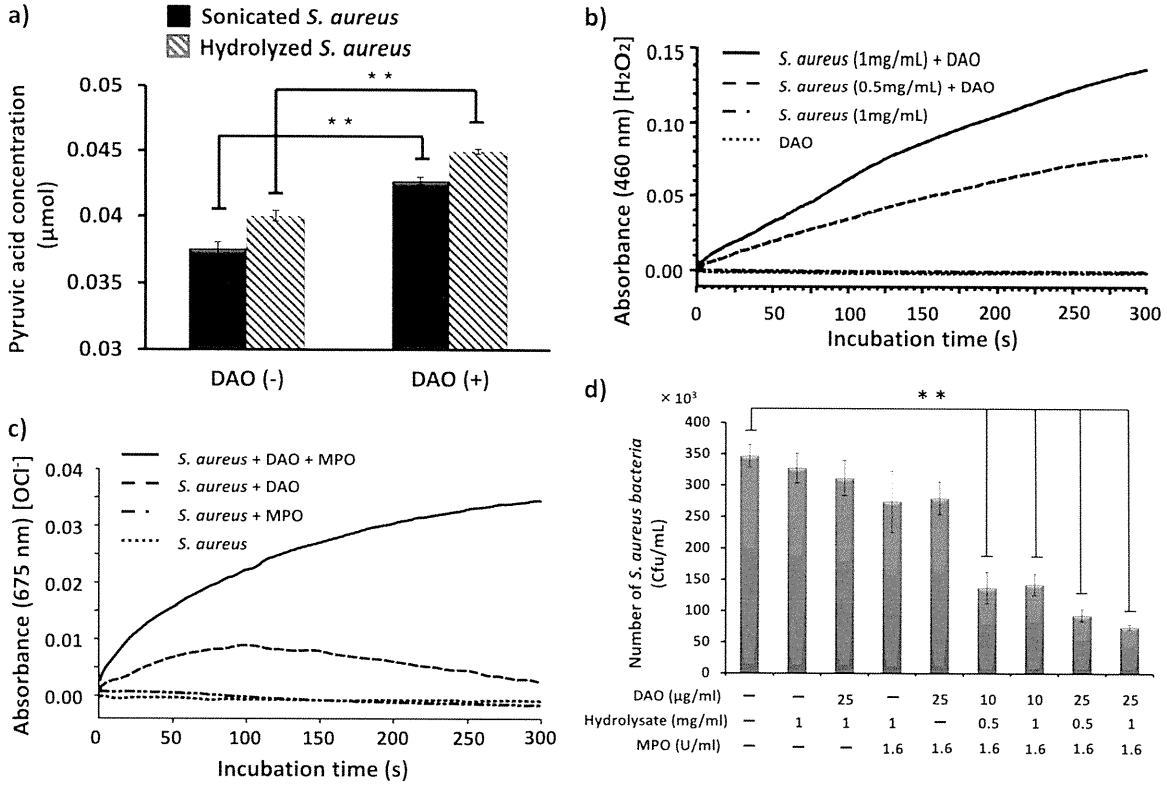

FIG 3 Utilization of bacterial cell wall-derived D-amino acid by DAO and generation of the bactericidal molecule HOCl. (a) Lysate of *S. aureus* (1 mg/ml) was incubated with 0.2 mg/ml DAO for 30 min at 37°C, and then pyruvic acid production was quantified as described in Materials and Methods. (b) Lysate of *S. aureus* (0.5 to 1 mg/ml) was incubated with DAO (5 μg/ml) in 50 mM phosphate buffer at 25°C for the indicated time to generate H_2O_2. H_2O_2 was measured by use of peroxidase-coupled oxidation of *o*-dianisidine (460 nm) as described in Materials and Methods. (c) Lysate of *S. aureus* (1 mg/ml) was incubated with DAO (200 μg/ml) plus MPO (1.6 U/ml) in the presence of SBT in acetate buffer (pH 5.5), and then absorbance at 675 nm was measured for HOCl generation. (d) *S. aureus* (1×10^6 CFU/ml) was incubated with the lysate of *S. aureus* (0.5 to 1.0 mg/ml), DAO (10 to 25 μg/ml), and MPO (1.6 U/ml) in 50 mM phosphate citrate buffer (pH 5.5) at 37°C for 30 min. Each reaction mixture was diluted with physiological saline, mixed with warm SCD agar, and plated on petri dishes. The bacterial colonies were counted after overnight culture at 37°C. The values are means and SD. **, statistically significant differences ($P < 0.01$) by Student's *t* test.

Difference in DAO activitin in $DAO^{+/+}$ and $DAO^{-/-}$ mice and their susceptibilities to bacterial infection. Certain ddY mice reportedly have a single-nucleotide substitution (541 G→A) in the *Dao* gene (Fig. 4a) (19). This nucleotide polymorphism results in the glycine (GGG)-to-arginine (AGG) amino acid substitution, which inactivates the enzyme activity of mouse DAO (19). We therefore sorted ddY mice into wild-type ($DAO^{+/+}$) and DAO-deficient ($DAO^{-/-}$) mice by using a restriction fragment length polymorphism (RFLP) method (Fig. 4b). Among 46 female ddY mice from Japan SLC, Inc., that were tested, 6 were wild-type mice (+/+), 16 were homozygous mutant mice (−/−), and 24 were heterozygous mice (+/−).

DAO activity in kidneys of ddY mice with different DAO expression levels was measured as described in Materials and Methods. Consistent with the results of *Dao* genotyping, DAO enzyme activity in the kidneys of $DAO^{+/+}$ mice was highest, and the lowest DAO activity occurred in kidneys of $DAO^{-/-}$ mice (56.9 mU/g wet tissue versus 0.04 mU/g wet tissue). $DAO^{+/-}$ mice showed about half the wild-type DAO activity (21.7 mU/g wet tissue) (Fig. 4c). To investigate the susceptibilities of mice with different DAO expression levels, ddY mice were injected intravenously (i.v.) with *S. aureus* via the tail vein as a renal bacterial infection model, and the number of viable bacteria in the kidneys was determined. The numbers of viable bacteria in the kidneys of the $DAO^{+/+}$ and $DAO^{+/-}$ mice were significantly reduced (to about 10%) compared with the numbers in the kidneys of $DAO^{-/-}$ mice (Fig. 4d). No significant difference was seen between $DAO^{+/+}$ and $DAO^{+/-}$ mice. We also examined the survival rate of ddY mice infected with *S. aureus*. After 2 weeks, 2 of 9 $DAO^{-/-}$ mice survived, whereas 5 of 9 $DAO^{+/+}$ mice survived (Fig. 4e).

DAO activity and bactericidal activity of neutrophils derived from DAO variant mice. We also examined the DAO activity of peritoneal neutrophils derived from $DAO^{+/+}$ and $DAO^{-/-}$ mice. The DAO activity of neutrophils derived from $DAO^{-/-}$ mice was 9.4 μU/mg protein, whereas that of neutrophils derived from $DAO^{+/+}$ mice was 125 μU/mg protein (Fig. 5a). Incubation with mouse peritoneal neutrophils dramatically reduced the viability of *S. aureus*, although no significant difference was seen between $DAO^{+/+}$ and $DAO^{-/-}$ mice (Fig. 5b).

DISCUSSION

In our previous studies, we reported that DAO showed selective cytotoxicity against various cancer cells *in vitro* and *in vivo* (12, 13). DAO-mediated cytotoxicity was nullified by the addition of catalase, which suggested that DAO exerted cytotoxic effects via production of H_2O_2. In this study, we examined the potential bacteriostatic and bactericidal activities of DAO *in vitro* and *in vivo*, as well as the role of DAO in MPO-dependent killing. For this

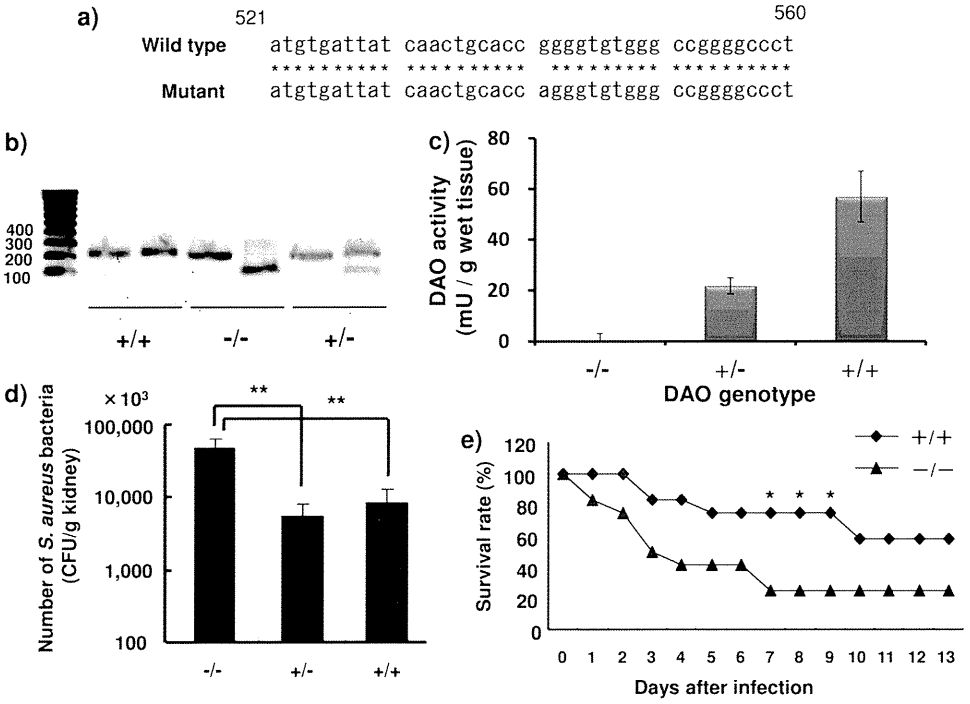

FIG 4 The *Dao* variant gene in ddY mice and its role in bacterial infection. (a) DNA sequences of the *Dao* genes in wild-type ($DAO^{+/+}$) and mutant ($DAO^{-/-}$) mice. Asterisks indicate identical nucleotide sequences. (b) The mouse *Dao* gene was amplified via a pair of 5′-mDAO and 3′-mDAO primers, followed by digestion with PflMI restriction enzyme. These digested fragments were applied to gel electrophoresis in a 1% agarose gel. (c) DAO activity in kidney homogenates was measured as described in Materials and Methods. (d) Fate of *S. aureus* after injection of 1×10^7 CFU/mouse. Three days after i.v. bacterial infection, viable bacteria in kidney homogenates were counted as described in Materials and Methods ($n = 7$ to 8). The values are means and SD. **, statistically significant differences ($P < 0.01$) by Student's *t* test. (e) Female ddY mice, 6 weeks old, were injected with *S. aureus*, 1×10^8 CFU/mouse, via the tail vein. The survival rates of the $DAO^{+/+}$ and $DAO^{-/-}$ groups were checked daily ($n = 9$). *, statistically significant differences ($P < 0.05$) by the chi-square test.

purpose, we prepared recombinant DAO obtained from different sources (i.e., pig, mouse, and human). We found that porcine DAO yielded both more DAO and higher enzyme activity than did the other DAOs (data not shown). We therefore utilized recombinant porcine DAO for our *in vitro* study. The recombinant DAO showed a single band, as judged from an SDS-PAGE gel stained with Coomassie brilliant blue. The relative activity of recombinant DAO was 5.3 U/mg protein, which is equivalent to that of purified DAO from porcine kidney.

In the present study, we observed that in the presence of 10 mM D-Ala, DAO showed concentration-dependent bacteriostatic activity against *S. aureus*, with the 50% inhibitory concentration (IC_{50}) of DAO almost 2 μg/ml (Fig. 1a). In the presence of 2 μg/ml of DAO, D-Ala showed a concentration-dependent bacteriostatic effect, and incubation of *S. aureus* with more than 5 mM D-Ala completely suppressed bacterial growth (Fig. 1b). Such DAO-mediated bacteriostatic activity was abolished by addition of catalase (Fig. 1c). This result clearly indicates the important role of H_2O_2 in the bacteriostatic activity of DAO. In this setting, L-Ala, D-Glu, and D-Asp did not show any bacteriostatic activity toward *S. aureus* even in the presence of DAO (Fig. 1a and d). This is because L-Ala, D-Glu, and D-Asp are not preferred substrates for DAO, and thus, there was no production of H_2O_2. D-Pro, which is a preferable substrate for DAO, showed more potent bacteriostatic activ-

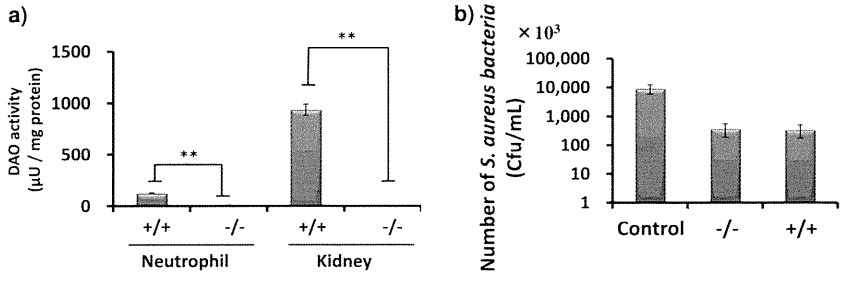

FIG 5 DAO activity of mouse peritoneal neutrophils and antibacterial activity of $DAO^{-/-}$ and $DAO^{+/+}$ mouse peritoneal neutrophils. (a) Peritoneal neutrophils were elicited using 6% casein sodium salt. The DAO activities of mouse neutrophils and kidney were measured, as evaluated by pyruvic acid formation. (b) *S. aureus* (4×10^6 CFU/ml) was incubated with or without equal numbers of mouse peritoneal neutrophils (1:1) at 37°C for 30 min. Serial dilutions were mixed with SCD agar on petri dishes, and the bacterial colonies were counted after overnight culture at 37°C. The values are means and SD. **, statistically significant differences ($P < 0.01$) by Student's *t* test.

ity against *S. aureus* (Fig. 1d and e). These results indicate that DAO needs available D-amino acids, such as D-Ala or D-Pro, to exhibit bacteriostatic activity.

Compared to the bacteriostatic activity of DAO, the bactericidal activity of D-Ala plus DAO was very weak (Fig. 2a and d);10 μg/ml DAO plus 5 mM D-Ala decreased the viable bacteria only to about 35%, at which point growth of *S. aureus* was completely suppressed (Fig. 1a and b). We further examined the bactericidal activity of the combination of DAO and MPO. MPO is an abundant protein in neutrophils (~5% of cellular protein) and is rich in granules (4). MPO is also found in the extracellular compartment after degranulation of granules (15). The biochemical function of MPO is oxidation of the Cl^- using H_2O_2 under acidic pH to produce HOCl. The resultant HOCl shows highly potent bactericidal activity (1).

In the present study, we showed that incubation of DAO and D-Ala with MPO in the presence of chloride ion at pH 5.5 generated HOCl (Fig. 2a). In this assay system, H_2O_2 was supplied via the reaction of DAO with D-Ala, after which MPO oxidized the chloride ion to generate HOCl. We then showed the bactericidal activity of DAO in combination with MPO. It was realized that MPO significantly enhanced the bactericidal activity of DAO when D-Ala or D-Pro was present (Fig. 2). Maximum bactericidal activity was observed when *S. aureus* was incubated with DAO, D-pro followed by D-Ala, and MPO; more than 99% of *S. aureus* bacteria were killed (Fig. 2c). Concerted bactericidal activity of DAO and MPO was not observed with the addition of L-Ala, D-Glu, or D-Asp (Fig. 2c and e) because these three amino acids are not preferable substrates for DAO reaction.

Peptidoglycan of *S. aureus* consists of alternating units of *N*-acetylglucosamine and *N*-acetylmuramic acid and a pentapeptide containing L-Ala, D-Ala, and D-Glu for structural integrity (28). D-Ala and D-Glu are generated by amino acid racemase and also by D-amino acid transaminase in bacteria (25). We next examined the availability of D-amino acids derived from bacteria for the substrate of DAO. By the incubation of bacterial lysate with DAO, the levels of pyruvic acid, a reaction product of DAO plus D-Ala, and H_2O_2 were elevated (Fig. 3a and b). Generation of H_2O_2 was observed by incubation of DAO and bacterial lysate, although the level of H_2O_2 was not sufficient to suppress the growth of *S. aureus* in SCD broth (data not shown). However, in the presence of MPO, concerted bactericidal activity against *S. aureus* was observed with DAO plus MPO and bacterial lysate. Namely, mixing of DAO (25 μg/ml), MPO (1.6 U/ml), and bacterial lysate (1 mg/ml) showed 80% killing of viable bacteria, whereas without MPO no bactericidal activity was observed (Fig. 3d). Thus, this bactericidal activity is thought to be mediated by the generation of HOCl (Fig. 3c). In fact, according to the literature, the culture medium of *S. aureus* contains D-amino acids at the mM level. The availability of D-Ala for DAO to utilize for the generation of H_2O_2 is considered to come from *de novo*-synthesized (by racemase) D-Ala. Importantly, DAO and MPO reportedly bind to bacterial cell walls and exhibit bacteriostatic and bactericidal activities (2, 29). This cell wall-binding property is advantageous for more localized and concentrated generation of antibacterial molecules, such as H_2O_2 and HOCl (2, 29). These results thus indicate that DAO and MPO can act synergistically in an antibacterial system.

Konno and Yasumura reported genetic polymorphism in the *Dao* gene in ddY mice (19). A fraction of ddY mice possess a single-nucleotide polymorphism in the *Dao* gene: a nucleotide change from GGG to AGG, which causes a glycine-to-arginine amino acid substitution. This amino acid substitution disrupted DAO enzyme activity without affecting the DAO expression level (19). We thus grouped ddY mice on the basis of genetic polymorphism by using the RFLP method, as described previously. Of 46 female ddY mice, 16 were double mutants ($DAO^{-/-}$), 24 were heterozygous ($DAO^{+/-}$), and 6 were wild type ($DAO^{+/+}$). In agreement with genotyping of the *Dao* gene, $DAO^{-/-}$ mice showed the lowest DAO activity (0.04 mU/g wet tissue) and $DAO^{+/+}$ mice had the highest DAO activity (56.9 mU/g wet tissue). $DAO^{+/-}$ mice had almost half the DAO activity (21.7 mU/g wet tissue) of $DAO^{+/+}$ mice.

We also examined the antibacterial role of DAO in an *in vivo* setting using $DAO^{+/+}$ and $DAO^{-/-}$ mice. Intravenous injection of *S. aureus* resulted in severe renal infection. Compared with $DAO^{-/-}$ mice, $DAO^{+/+}$ mice had significantly reduced (to less than 10%) numbers of viable bacteria in the kidney (Fig. 4d). Consistent with this result, $DAO^{+/+}$ mice demonstrated greater resistance to *S. aureus* infection (i.e., had a higher survival rate) than $DAO^{-/-}$ mice (Fig. 4e).

The neutrophil is one of the most important defenses against microbial infection, and its dysfunction causes severe chronic infection (3, 17). Therefore, we examined whether neutrophils derived from $DAO^{-/-}$ mice had lower bactericidal activity than neutrophils derived from $DAO^{+/+}$ mice. In fact, peritoneal neutrophils derived from $DAO^{+/+}$ mice showed higher DAO activity than did those derived from $DAO^{-/-}$ mice (Fig. 5a). However, contrary to our expectation, no difference in bactericidal activity was observed for neutrophils derived from $DAO^{+/+}$ and those derived from $DAO^{-/-}$ mice (Fig. 5b). This result may be due to the relatively low H_2O_2 generation potential of DAO compared with NADPH oxidase, which is the major source of H_2O_2 in neutrophils. DAO may not affect the net amount of H_2O_2 in neutrophils, and thus, it may not be the primary antibacterial component in neutrophils. However, it may be one component operating in antimicrobial defense, which may become important in specific cases, for example, NADPH oxidase deficiency. As mentioned above, DAO activity was higher in the kidneys of $DAO^{+/+}$ and $DAO^{+/-}$ mice, about 56.9 mU/g wet tissue and 21.7 mU/g wet tissue, respectively, than in $DAO^{-/-}$ mice. This activity is thought to be enough to reduce bacterial growth in the kidney, because a DAO concentration of 10 μg/ml suppressed bacterial growth, as shown in Fig. 1a and b. However, we could not show direct evidence that kidney homogenates exhibit bactericidal activity toward *S. aureus* (data not shown). This may be because, in this experimental workup, cellular integrity was completely destroyed, and formation of a phagosome and accumulation of antibacterial protein and supply of D-Ala at a localized site were not complete enough to show bactericidal activity, although more studies are needed to confirm this possibility. In this regard, Zhang et al. reported the potential binding of DAO to bacterial cell walls, and DAO showed higher antibacterial activity than a theoretical amount of H_2O_2, as calculated from the unit activity of DAO (30). Such H_2O_2 generation in the vicinity of bacteria may be advantageous for avoiding H_2O_2 degradation by kidney catalase before the H_2O_2 can act against the bacteria. Furthermore, neutrophils are recruited to the infected site, and abundant MPO may be available at sites of bacterial infection, which can exert the synergistic effect of DAO with MPO. In fact, in this study, we found that $DAO^{+/+}$

mice had less infection in the kidney and a higher survival rate after intravenous infection with *S. aureus* than $DAO^{-/-}$ mice.

S. aureus, used in the present study, is a catalase-producing bacterium and so is able to degrade H_2O_2 to water and oxygen. Production of catalase is well correlated with susceptibility to hydrogen peroxide treatment and with virulence and survival in the polymorph nuclear phagocyte (16, 22), though catalase-negative *S. aureus* may be more susceptible to treatment with DAO, D-Ala, and MPO, which remains to be elucidated. We also noticed that catalase-negative bacteria, such as *Streptococcus* spp., were more resistant to hydrogen peroxide treatment and DAO treatment (data not shown). This may be due to other anti-ROS enzymes, such as peroxidases, filling the role of catalase (6).

Based on the results shown in Fig. 1 and 2, DAO requires free D-amino acids, such as D-Ala or D-Pro, in order to exert bacteriostatic and bactericidal activities. Two D-amino acid sources of supply may be available in the *in vivo* setting: the infecting and growing bacteria and the enterobacteria. It has been reported that *S. aureus* possesses DAO-reactive materials, free D-amino acid, in the cell pool at 3.6 μmol/100 mg (dry weight) of cells (5). Also, approximately 1 mM D-amino acids are secreted from bacteria in the bacterial culture medium (20). Konno et al. observed that the D-amino acids that accumulated in urine and tissues derived from enterobacteria in $DAO^{-/-}$ mice, but not in normal mice, which indicates that DAO continuously catabolizes D-amino acids and thus generates H_2O_2 by means of endogenously derived D-amino acids in the kidney or other tissues (18). These possibilities remain to be elucidated.

These observations suggest that DAO exhibits bacteriostatic activity and bactericidal activity in the presence of MPO *in vitro*. The substrate of DAO, D-amino acids, may be supplied from infecting bacteria or endogenous bacteria *in vivo* to some extent. Thus, DAO, in combination with MPO, may be an antibacterial system in mammals, especially in the kidney but perhaps also in the lung and liver, which utilizes D-amino acids derived from endogenous bacteria in infections.

ACKNOWLEDGMENT

This work was supported by Grant-in-Aid for Scientific Research 21791016 from the Ministry of Education, Culture, Sports, Science and Technology of Japan.

REFERENCES

1. **Albrich JM, McCarthy CA, Hurst JK.** 1981. Biological reactivity of hypochlorous acid: implications for microbicidal mechanisms of leukocyte myeloperoxidase. Proc. Natl. Acad. Sci. U. S. A. **78**:210–214.
2. **Allen RC, and Stephens JT, Jr.** 2011. Myeloperoxidase selectively binds and selectively kills microbes. Infect. Immun. **79**:474–485.
3. **Baehner RL, Nathan DG, Karnovsky ML.** 1969. The metabolic and bactericidal defect in chronic granulomatous disease. Vox Sang. **17**:35–36.
4. **Bainton DF, Ullyot JL, Farquhar MG.** 1971. The development of neutrophilic polymorphonuclear leukocytes in human bone marrow. J. Exp. Med. **134**:907–934.
5. **Bhattacharyya SK, Banerjee AB.** 1974. D-Amino acids in the cell pool of bacteria. Folia Microbiol. **19**:43–50.
6. **Brenot A, King KY, Janowiak B, Griffith O, Caparon MG.** 2004. Contribution of glutathione peroxidase to the virulence of Streptococcus pyogenes. Infect. Immun. **72**:408–413.
7. **Briggs RT, Karnovsky ML, Karnovsky MJ.** 1977. Hydrogen peroxide production in chronic granulomatous disease. A cytochemical study of reduced pyridine nucleotide oxidases. J. Clin. Invest. **59**:1088–1098.
8. **Chumakov I, et al.** 2002. Genetic and physiological data implicating the new human gene G72 and the gene for D-amino acid oxidase in schizophrenia. Proc. Natl. Acad. Sci. U. S. A. **99**:13675–13680.
9. **Clifford DP, Repine JE.** 1982. Hydrogen peroxide mediated killing of bacteria. Mol. Cell Biochem. **49**:143–149.
10. **Cline MJ, Lehrer RI.** 1969. D-Amino acid oxidase in leukocytes: a possible D-amino-acid-linked antimicrobial system. Proc. Natl. Acad. Sci. U. S. A. **62**:756–763.
11. **D'Aniello A, et al.** 1993. Biological role of D-amino acid oxidase and D-aspartate oxidase. Effects of D-amino acids. J. Biol. Chem. **268**:26941–26949.
12. **Fang J, et al.** 2008. Oxystress inducing antitumor therapeutics via tumor-targeted delivery of PEG-conjugated D-amino acid oxidase. Int. J. Cancer **122**:1135–1144.
13. **Fang J, Sawa T, Akaike T, Maeda H.** 2002. Tumor-targeted delivery of polyethylene glycol-conjugated D-amino acid oxidase for antitumor therapy via enzymatic generation of hydrogen peroxide. Cancer Res. **62**:3138–3143.
14. **Haase LW.** 1950. Bactericidal action of hydrogen peroxide, peroxides, and oxidizing compounds. Pharmazie **5**:436–437.
15. **Jaovisidha P, Peeples ME, Brees AA, Carpenter LR, Moy JN.** 1999. Respiratory syncytial virus stimulates neutrophil degranulation and chemokine release. J. Immunol. **163**:2816–2820.
16. **Kanafani H, Martin SE.** 1985. Catalase and superoxide dismutase activities in virulent and nonvirulent Staphylococcus aureus isolates. J. Clin. Microbiol. **21**:607–610.
17. **Klebanoff SJ, White LR.** 1969. Iodination defect in the leukocytes of a patient with chronic granulomatous disease of childhood. N. Engl. J. Med. **280**:460–466.
18. **Konno R, Niwa A, Yasumura Y.** 1990. Intestinal bacterial origin of D-alanine in urine of mutant mice lacking D-amino-acid oxidase. Biochem. J. **268**:263–265.
19. **Konno R, Yasumura Y.** 1983. Mouse mutant deficient in D-amino acid oxidase activity. Genetics **103**:277–285.
20. **Lam H, et al.** 2009. D-Amino acids govern stationary phase cell wall remodeling in bacteria. Science **325**:1552–1555.
21. **Lyle LR, Jutila JW.** 1968. D-Amino acid oxidase induction in the kidneys of germ-free mice. J. Bacteriol. **96**:606–608.
22. **Mandell GL.** 1975. Catalase, superoxide dismutase, and virulence of Staphylococcus aureus. In vitro and in vivo studies with emphasis on staphylococcal-leukocyte interaction. J. Clin. Invest. **55**:561–566.
23. **Nagata Y, Yamada R, Nagasaki H, Konno R, Yasumura Y.** 1991. Administration of D-alanine did not cause increase of D-amino acid oxidase activity in mice. Experientia **47**:835–838.
24. **Paul BB, Strauss RR, Jacobs AA, Sbarra AJ.** 1970. Function of H(2)O(2), myeloperoxidase, and hexose monophosphate shunt enzymes in phagocytizing cells from different species. Infect. Immun. **1**:338–344.
25. **Pucci MJ, Thanassi JA, Ho HT, Falk PJ, Dougherty TJ.** 1995. Staphylococcus haemolyticus contains two D-glutamic acid biosynthetic activities, a glutamate racemase and a D-amino acid transaminase. J. Bacteriol. **177**:336–342.
26. **Robinson JM, Briggs RT, Karnovsky MJ.** 1978. Localization of D-amino acid oxidase on the cell surface of human polymorphonuclear leukocytes. J. Cell Biol. **77**:59–71.
27. **Sakamoto R, et al.** 2003. A new water-soluble chromogenic indicator: an application to the determination of chlorine in aqueous solutions. Anal. Sci. **19**:1445–1447.
28. **Schleifer KH.** 1975. Chemical structure of the peptidoglycan, its modifiability and relation to the biological activity. Z. Immunitatsforsch. Exp. Klin. Immunol. **149**:104–117.
29. **Zhang H, Yang Q, Sun M, Teng M, Niu L.** 2004. Hydrogen peroxide produced by two amino acid oxidases mediates antibacterial actions. J. Microbiol. **42**:336–339.
30. **Zhang M, et al.** 2011. Behavioral characterization of a mutant mouse strain lacking D-amino acid oxidase activity. Behav. Brain Res. **217**:81–87.

PROCEEDINGS
OF THE
JAPAN ACADEMY
SERIES B
PHYSICAL AND BIOLOGICAL SCIENCES

Proc. Jpn. Acad., Ser. B, Vol. 88, 53–71 (2012)

Vascular permeability in cancer and infection as related to macromolecular drug delivery, with emphasis on the EPR effect for tumor-selective drug targeting

Hiroshi MAEDA

Review

Vascular permeability in cancer and infection as related to macromolecular drug delivery, with emphasis on the EPR effect for tumor-selective drug targeting

By Hiroshi MAEDA[*1,†]

(Communicated by Takashi SUGIMURA, M.J.A.)

Abstract: Tumor and inflammation have many common features. One hallmark of both is enhanced vascular permeability, which is mediated by various factors including bradykinin, nitric oxide (NO), peroxynitrite, prostaglandins etc. A unique characteristic of tumors, however, is defective vascular anatomy. The enhanced vascular permeability in tumors is also distinctive in that extravasated macromolecules are not readily cleared. We utilized the enhanced permeability and retention (EPR) effect of tumors for tumor selective delivery of macromolecular drugs. Consequently, such drugs, nanoparticles or lipid particles, when injected intravenously, selectively accumulate in tumor tissues and remain there for long periods. The EPR effect of tumor tissue is frequently inhomogeneous and the heterogeneity of the EPR effect may reduce the tumor delivery of macromolecular drugs. Therefore, we developed methods to augment the EPR effect without inducing adverse effects for instance raising the systemic blood pressure by infusing angiotensin II during arterial injection of SMANCS/Lipiodol. This method was validated in clinical setting. Further, benefits of utilization of NO-releasing agent such as nitroglycerin or angiotensin-converting enzyme (ACE) inhibitors were demonstrated. The EPR effect is thus now widely accepted as the most basic mechanism for tumor-selective targeting of macromolecular drugs, or so-called nanomedicine.

Keywords: enhanced permeability and retention (EPR) effect, infection and cancer, nanomedicine, vascular permeability, tumor targeted drug delivery, nitric oxide/super oxide

1. Introduction

In the 1980s–1990s, we demonstrated a mechanism that mediates extravasation upon bacterial infection via the activation of protease cascades involving kallikrein system that generates bradykinin (kinin).[1)–6)] Subsequently we found a similar cascade of kinin generation did involve in vascular permeability in the solid tumor.[7)–10)] Concomitant generation of nitric oxide (NO) was also discovered. Then prostacyclins were also found involved in vascular permeability in solid tumors as was also the case in inflamed tissues.[11)–16)]

This finding was important because of our interest of drug delivery to solid tumor using macromolecular drugs, more specifically polymer [SMA] conjugated neocarzinostatin [NCS] designated as SMANCS.[17),18)] SMA is a synthetic polymer of styrene-co-maleic acid of about 1.2 KDa with high lipophilicity, which was covalently conjugated to NCS via amide bond. SMA also conferred albumin binding capacity to SMANCS, as well as quite different pharmacological properties *in vivo*. Using this polymer conjugate macromolecular drug SMANCS, we found its remarkable accumulation in the tumor tissue. Then we clarified that it was extravasated more selectively in solid tumor as was a case observed by bacterial infected site where blue albumin was extravasated due to kinin generation.[8)–10)]

Because of the high lipophilicity of SMANCS we also found that it could be solubulized in lipid contrast agent [Lipiodol®] (SMANCS/Lipiodol) (see

*1 Institute of Drug Delivery System Research, School of Pharmaceutical Sciences, Sojo University, Kumamoto, Japan.

† Correspondence should be addressed: H. Maeda, Professor, Institute of Drug Delivery System Research, School of Pharmaceutical Sciences, Sojo University, 4-22-1 Ikeda, Kumamoto 860-0082, Japan (e-mail: hirmaeda@ph.sojo-u.ac.jp).

doi: 10.2183/pjab.88.53

discussion later). We further found that arterial injection of Lipiodol, or SMANCS/Lipiodol truly targeted tumor tissue selectively.[19),20)] There was no other method that can target an anticancer agent with so much selectively.

In this review article, I will therefore discuss the unique vascular pathophysiology, microanatomy of tumors and the biochemical mechanisms involved in the enhanced permeability and retention (EPR) effect. More important, I also describe how we can augment the tumor selective drug delivery and hence improve the therapeutic efficacy using macromolecular anticancer drugs—the issue of greatest importance that addressed in this article.

2. Tumor selective macromolecular drug, SMANCS, and lipid formulation for arterial infusion; The method for pin-pointed tumor delivery

Following the structural study of proteinaceous antitumor agent neocarzinostatin, or NCS, we synthesized a polymer (SMA) conjugated derivative of NCS, designated SMANCS in 1978.[17),18)] The main objective was to develop a drug that would accumulate in the lymphatic system utilizing SMA-component that would confer lipophilic as well as and macromolecular nature. In lymphology macromolecules or lipidic particle are known to be recovered via the lymphatic system.[21)] Therefore, a lymphotropic drug would be preferred character to deliver the drug to the lymphatics system, thus ideal drug against lymphatic metastasis.[22),21)] That is one of the major problems in cancer treatment.

When SMANCS dissolved in water was injected intravenously, it was accumulated predominantly in the lymph nodule.[23)] Furthermore, because of its lipophilic nature of SMANCS, I found it could be dissolved in the lipid contrast agent (Lipiodol®, iodinated poppy seed oil ethyl ester). In collaboration with Toshimitsu Konno, Surgery Department, Kumamoto University, we pursued arterial infusion of SMANCS/Lipiodol (SX/LP) into the tumor feeding artery of VX-2 tumor implanted in the rabbit liver to facilitate more tumor targeted delivery. When SMANCS/Lipiodol was infused into the hepatic artery, extraordinary high intratumor concentration was found. Namely the drug concentration in the tumor compared to that of blood was more than 2000 fold in the tumor.[19)] This pharmacological data of tumor uptake using SMANCS/Lipiodol was so remarkable, we pursued for its clinical development.

In the clinical front then, we had many advanced hepatoma patients in our hospital, and Professor Ikuzo Yokoyama of Department Surgery decided to undertake the evaluation of SX/LP for treatment of primary hepatoma, which exhibition unprecedented targeting and therapeutic response in VX-2 tumor. The method not only offers truly pin-point targeting drug delivery, but it also offers diagonostic information, such as exact tumor size, location, intrahepatic spread, and amount of drug delivered to tumor because the remaining of Lipiodol could be clearly detected by X-ray CT-scan.[24)–26)] This was the first example of theranostic modality in early 1980s, which is now becoming popular. This therapeutic method using SMANCS was later approved for hepatoma treatment in 1993 by the Japanese Government.

3. Discovery of the EPR effect of macromolecules in solid tumors and its elaboration

We first observed prolonged tumor-selective accumulation of blue albumin (67 kDa) (Fig. 1A,B), which can be readily visualized by injecting Evans blue intravenously as a blue tumor.[27)] The amount of Evans blue-albumin in the tumor and other organs were quantified, and time dependent progressive accumulation was only seen in the tumor tissues (Fig. 2A). The tumor concentration of blue albumin was about 10 fold higher than that of blood at 145 hrs (Fig. 2A). This phenomenon was coined the enhanced permeability and retention (EPR) effect. We also confirmed the EPR effect by using radiolabeled serum proteins; IgG (170 kDa), transferrin (90 kDa), albumin (67 kDa), and ovalbumin (48 kDa). However, we did not observe the EPR effect with low molecular weight proteins such as ovomucoid (29 kDa) and neocarzinostatin (12 kDa).[27)]

To confirm the molecular weight dependency of the EPR effect, we used biocompatible synthetic copolymers of hydroxypropyl methacrylate (HPMA), which ranged in size from 4.5 to 800 kDa,[28)–31)] that was kindly provided by Professors Karel Ulbrich and Ruth Duncan. We reconfirmed our earlier findings: most biocompatible plasma proteins and HPMA polymers between 4.5 and 800 kDa exhibited the EPR effect (Fig. 3A,B).[28)–33)] A more detailed time course study showed that the tumor uptake of HPMA copolymers after intravenous injection was relatively rapid: some showed a marked tumor uptake within a few hours, while smaller HPMA copolymers, about 30 kDa or smaller, showed no EPR effect. Figure 3B illustrates the relationship among tumor uptake, plasma concentration, and renal

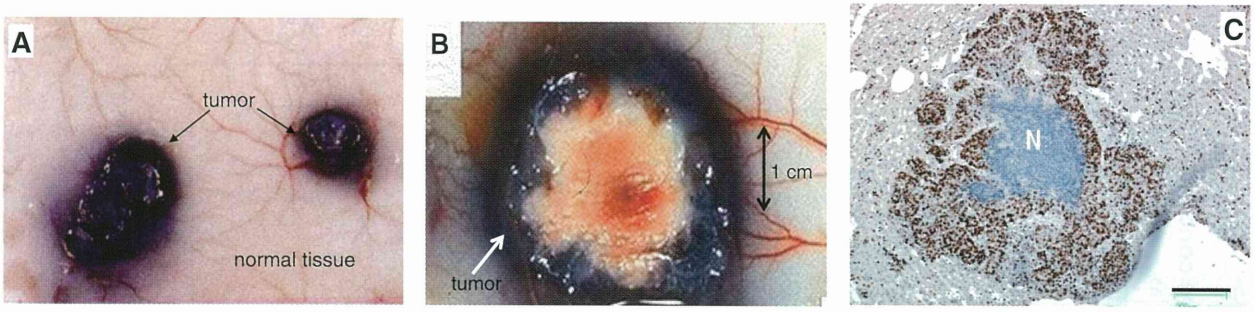

Fig. 1. (A and B): Extravasation of Evans blue-bound albumin in S-180 tumor in mice. Blue staining (extravasation) is homogeneous in A, but heterogeneous in B. Note the lack of leakage in the normal skin tissue in the background in A and B. (C) Heterogeneity of a micro tumor nodule at microscopic level (Ki-67 immunohistochemistry/DAB staining for viable cells: brown, ×100).[44] Note central portion of the nodule is necrotic (N) and the periphery is viable. Nodule size is about 0.5 mm in diameter. The tumor used was methylhydrazine-induced colon cancer in inbred CBA mice that was implanted in the spleen and allowed to metastasize to the liver (See refs. 35), 44), 84)).

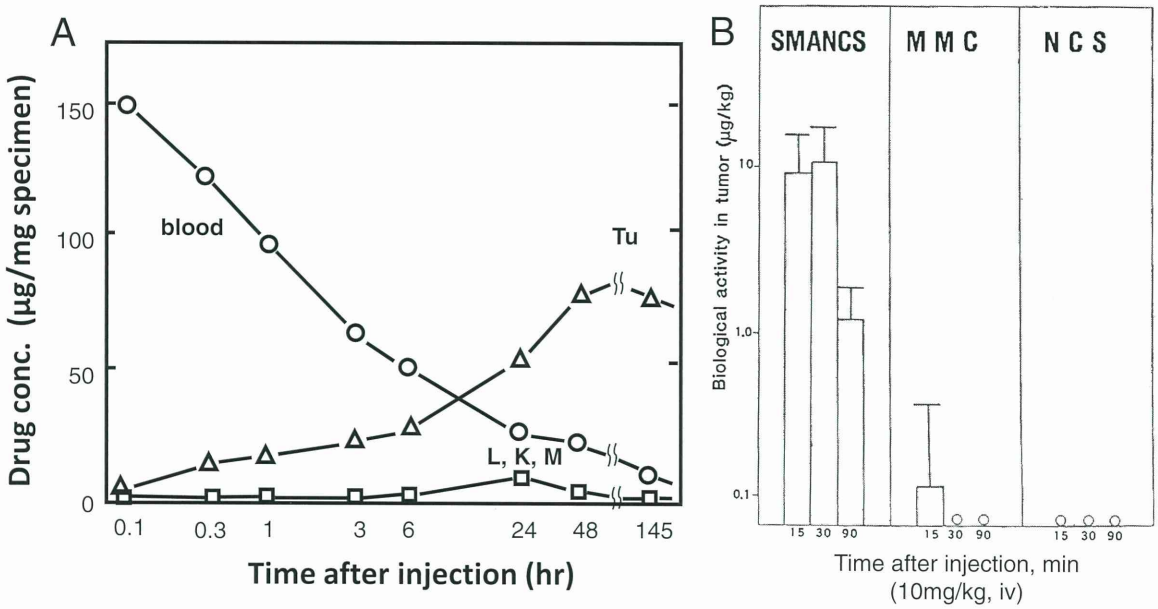

Fig. 2. (A) Quantitation of time dependent accumulation of Evans blue/albumin; in the tumor, blood and normal tissues (L, liver; K, kidney and M, muscle) (from ref. 27)). Evans blue (10 mg/kg) was injected i.v. and it will bind to plasma albumin. Levels of Evans blue in the blood and in the tumor (S-180 in mice) were inversely related, as the plasma level decreased, the tumor concentration increased. After 100 h or more, the T/B was about 10; ratios for normal tissues such as the liver (L), kidney (K), and muscle (M) to tumor were less than 1/40. (B) Tumoritropic accumulation of macromolecular anticancer agent SMANCS, and low molecular weight drugs mitomycin [MMC] and the parental drug neocarzinostatin [NCS] at different time point; at 15, 30, and 90 min in S-180 tumor in mice.

clearance in terms of drug size (MW). A relatively long circulation time after intravenous injection was needed for the EPR effect to occur. For progressive drug accumulation to tumor, high drug concentrations in circulation is needed. For albumin and transferrin (not shown), the T/B becomes much higher after 6 h or more (Fig. 2A).[27)–30)] Once these macromolecules accumulate in solid tumor tissues, they are not cleared within a few days or weeks, in contrast to the situation in normal tissue. Biocompatible proteins and lipid particles are known to be removed from normal tissues via the lymphatic system in just days, however.[19)–22),27)] The prolonged retention time of macromolecular drugs in tumor tissue is thus another important aspect of the EPR effect.[27),34)–36)]

The upper size limit of macromolecular drugs exhibiting the EPR effect is actually quite large.

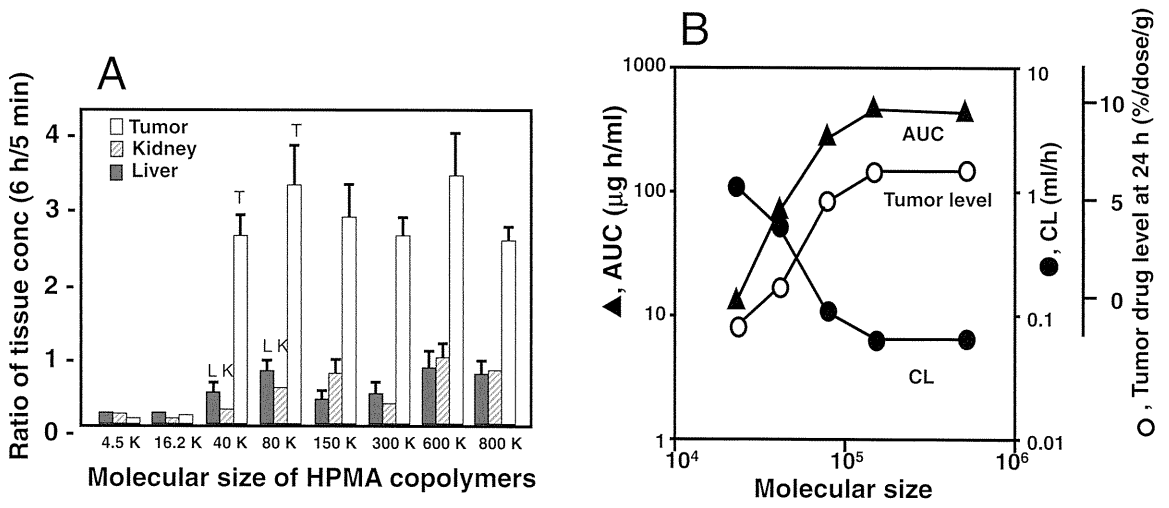

Fig. 3. Tumortropic uptake of biocompatible macromolecule HPMA (see text for detail). (A) The EPR effect is seen with HPMA copolymers (>40 kDa): tumor (□) compared to the liver (■) and the kidney (▨). Amount of tumor uptake is compared with 6h to that of 5 min. (B) Relationship between molecular sizes of putative polymeric drugs (HPMA) and their plasma levels (AUC, area under the concentration-time curve, ▲), tumor uptake, ○, and renal clearance rate (CL, ●) (Adapted from Noguchi *et al.*[28]).

Kimura *et al.*[37] showed earlier that *Lactobacillus* sp., 1–2 μm in size, accumulated more in tumor tissue than in normal. Recently, Zao *et al.* and Hoffman[38),39] showed that *Salmonella typhimurium* also preferentially accumulated in tumor compared with normal tissue. Konerding *et al.*[40] and Hashizume *et al.*[41] examined tumor vasculature and found that endothelial openings in the vessels could be as large as 4.7 μm (a mean of 1.7 μm) (Fig. 4D vs H) (see Section 4) which are not found in the normal vasculature. These results indeed agree well with the observation noted above that bacteria preferentially accumulated in tumor tissues after intravenous injection. Therefore the upper limit of molecular size to exhibit the EPR effect can be far greater than 10^6 Da, although the rate of intracellular uptake of such large molecules may not be as fast as that for 100-kDa.

With regard to the detection and imaging the tumor based on the uptake of low molecular weight radio contrast agents, which was infused into a tumor-feeding artery, we observed tumor staining lasted only short time (<1 min) in the angiogram. Tumors such as hepatoma and renal cell carcinoma can take up the contrast agent more efficiently than do normal tissues, resulting more tumor-selective staining, and hence detection. However, such X-ray images using an low MW contrast agent will disappear within 10 s or so because of rapid diffusion of the contrast agent. This type of tumor selective imaging may be called *passive targeting*, but such passive targeting has little value for therapeutic purpose, because conventional low MW anticancer agents also disappear within a few minutes or so.

What I emphasize here is that prolonged retention of drugs in tumor is critically important for therapeutic purpose, and that such retention is possible primarily with macromolecular or lipidic drugs. Arterial infusion of SMANCS/Lipiodol can aid tumor-selective imaging as well as drug delivery.[19)–22),36]

4. Microanatomy of tumor blood vessels and extravasation of macromolecular drugs: the cause of EPR effect

Morphology of blood vasculature in tumors and normal tissues is uniquely different. Microarchitecture of blood vessels can be visualized clearly by scanning electron microscopy (SEM) using vascular casts of plastic resin (Figs. 4A–H). Vascular image of metastatic liver cancer and colon cancer were elegantly described by Professor Paul E. O'Brien and his associates of the University of Melbourne[42)–44] (Fig. 4 A/B, normal, and E/F, tumor), and by Professor Moritz Konerding of the University of Mainz (Fig. 4 D/E, normal, and G/H, tumor)[40] respectively. One can notice a great contrast to the normal blood vasculature in Fig. 4 A/B (liver), C/D (colon) on the top vs tumor vasculature on the bottom (E–H). The metastatic tumor micronodule

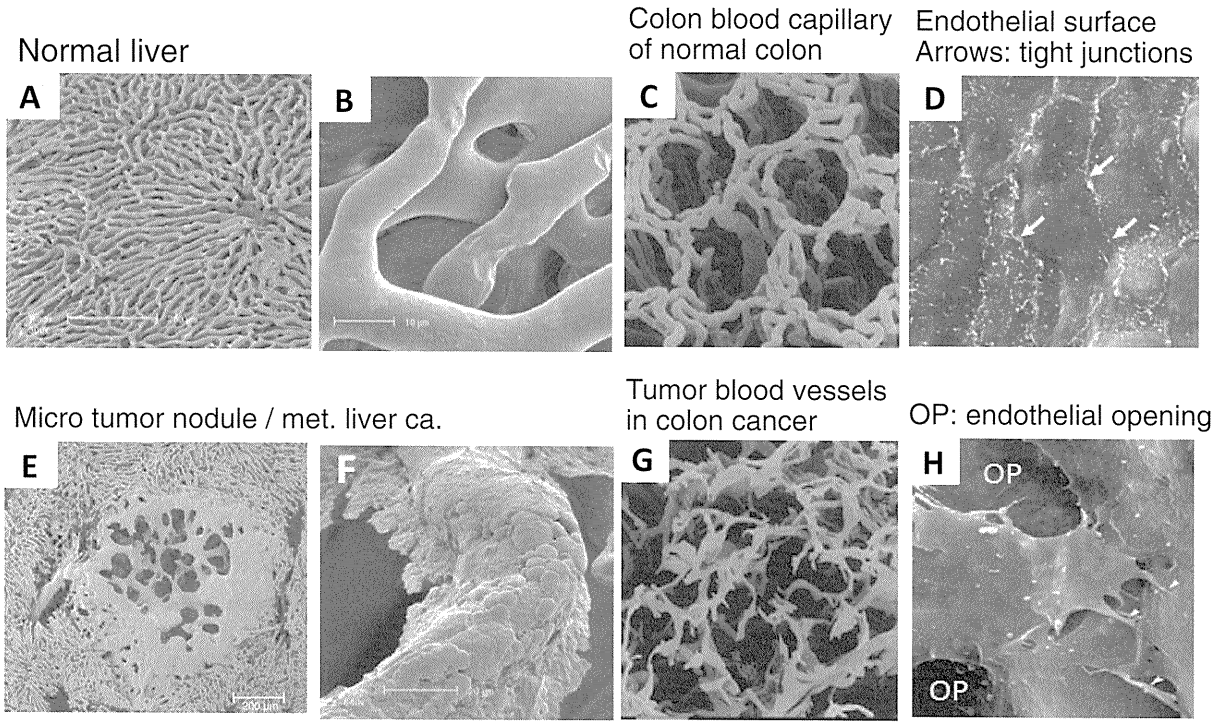

Fig. 4. Comparison of SEM images of blood vessels in normal healthy tissue (A–D on the top) and tumor tissues (E–H, lower figures) of metastatic tumor nodules in the liver from colon cancer. Blood vessels in healthy tissue in (A)–(C) show a clear, smooth, regular feature and no leakage of polymeric resin. In contrast the tumor vessels show polymer leakage (E) at the capillary level or in the early phase of leakage in (F). (See refs. 34), 35)). In (D) and (H) shown are SEM images of the luminal surface of normal blood vessel (D) which shows tight cell-cell junctions of endothelium, whereas blood vessels in the tumor (H) have large openings (OP in H) in the endothelium. (C) shows the vascular cast of normal colon with regularly shaped capillary, whereas an irregular vascular network can be seen in vascular cast of colon tumor (G) from ref. 36). (C), (D), (G), (H) courtesy of Prof. Konerding of Mainz.

in Fig. 4E is less than 0.5 mm in diameter, and it also demonstrates extravasation of the polymeric resin. This indicates clear architectural difference of neovasculature, compare with normal vessels. It should be noted that this neovasculature formation of tumor nodule is seen even as small as 200 μm, much smaller than the size reported by Folkman: size of 2–3 mm.[44)–47)] Konerding *et al.*[40)] demonstrated large endothelial openings at the luminal surface of tumor vessels (Fig. 4H), and a lack of discrete arteriole-capillary-venule systems (not shown), while revealing the tight cell-cell junctions of vascular endothelial cells in normal vessels (Fig. 4D). Tumor blood vessels also lack smooth muscle cell layer. These structural abnormalities and vascular permeability factors make tumor vessels more leaky than vessels in normal tissue. Polymer resin is being extravasated (Fig. 4E) into the tumor nodule, or in the beginning of leakage process to the outside of blood vessels (Fig. 4F). These extravasations did not occur in normal tissues. Further SEM images of vascular casts indeed demonstrate the facts of leakage of polymeric resin into tumor interstitium selectively, and a clear evidence of the defective functionality of tumor vessels. These defects make tumor vessels being highly permeable to albumin, IgG, and other macromolecules including the lipid contrast agent Lipiodol, and so called nanoparticles.[24)–36),42)–44)]

5. Factors involved in vascular permeability and the EPR effect in infection and solid tumors

5-1. Bradykinin. Kinin (bradykinin) is one of the most potent endogenous pain inducing nonapeptide, and it is continuously generated at sites of infection and cancer tissues by kallikrein and other proteases, from kininogen. However, it is degraded rapidly with a half-life ($t_{1/2}$) of a few seconds in plasma by host proteases such as kininase and angiotensin converting enzyme (ACE) *in vivo*.

We studied the vascular permeability of bacterial proteases with regard to the pathogenic mechanism in 1980s, and found that all bacterial proteases

activate one or more steps in the kallikrein-kinin cascade.[1)–4)] Thereby extravasation of plasma components occurs and edema ensues, which are events similar to those occurring in cancer. The kallikrein-kinin cascade is stimulated as a result of activated kallikrein (or Hageman factor/Factor XII and prekallikrein), or microbial proteases cleave off bradykinin directly from either high-molecular-weight or low-molecular-weight kininogen in the plasma[3)–11),13)] which causes pain and extravasation.

Most cancer cells produce various proteases, *e.g.*, serine-type proteases, cathepsins, and collagenases. These proteases are also involved in kinin production and thus result in vascular permeability enhancement (the EPR effect). We found that kinin also contributes to the formation of ascitic and pleural fluids in carcinomatosis. Kinin is thus a key factor in extravasation and accumulation of ascetic fluid in the peritoneal and pleural cavity.[7)–10)] Based on this fact, one can envision a relationship between kinin generation and clinical manifestations of pain in cancer patients similar event found in infection. However, very few studies on this issue have been undertaken, and investigation of kinin antagonists in cancer patients appears interesting.

Dvorak *et al.* reported vascular permeability factor (VPF) of peptide nature that was generated by cancer cells.[48),49)] Later it was found identical to the vascular endothelial growth factor (VEGF).[47),50)–53)] This means that neoangiogenesis of tumor tissue is reflecting other side of the same coin, vascular permeability, to supply nutrients for tumor growth.[52),53)]

5-2. Biological free radicals in vascular permeability in infection, cancer and related issues: ROS and RNS. ROS (reactive oxygen species), such as superoxide anion radical ($O_2^{\bullet-}$), and RNS (reactive nitrogen species) such as NO and peroxynitrite ($ONOO^-$) are induced in viral and bacterial infections. In influenza virus infection, we found that a critical cause of viral pneumonia was attributable to the excessive generation of $O_2^{\bullet-}$.[54)–56)] $O_2^{\bullet-}$ production was increased more than 300-fold in the lung or alveolar lavage fluid of the virus-infected mice compared with healthy control mice. The cause was attributable to the activation of xanthine oxidase (XO).[54)–56)] This finding indicates that ROS may be an important direct etiological agent in influenza infection. To confirm this possibility, we removed $O_2^{\bullet-}$ from the site of infection *in vivo* by using a pyran polymer-conjugated derivative of Cu, Zn-superoxide dismutase (SOD); this derivative showed a prolonged *in vivo* $t_{1/2}$ of SOD, and sustained enzyme activity. When the polymer conjugated SOD was injected, the disease severity was markedly reduced and the survival rate of mice was greatly improved, *i.e.*, 97% survived vs. 3% of the SOD non-treated group. When we augmented the production of $O_2^{\bullet-}$ by adding the substrate of XO, i.e., inosine or xanthine, however, the disease was severely exacerbated, and the survival rate of mice dropped more rapidly and to far greater extent compared with controls.[54),55)] Under the same experimental settings, we found that NO was generated in parallel with the production of $O_2^{\bullet-}$ in infection with influenza, herpes, and Sendai viruses and *Salmonella* sp. in mice.[57)–62)]

In our separate research, we had found that NO synthase (NOS) was highly expressed in a solid tumor, and demonstrated that NO facilitated the EPR effect.[11)–13),63)] Therefore, iNOS induction in infection would contribute vascular permeability. We[11)–13)] found in other studies that NO and $ONOO^-$ could facilitate the vascular permeability of solid tumor, with $ONOO^-$, which being a reaction product of NO and $O_2^{\bullet-}$ (*i.e.*, $NO + O_2^{\bullet-} \rightarrow ONOO^-$). Then $ONOO^-$ can activate pro-matrix metalloproteinases to generate active matrix metalloproteinases (proMMPs $\rightarrow$ MMPs or collagenase).[12)–14)] This collagenase also facilitated vascular permeability.[11)–13)] These three components (NO, $ONOO^-$, collagenase) can thus enhance the vascular permeability of normal blood vessels as well as tumor blood vessels, as described below.

Investigations in the same line of research revealed that $ONOO^-$, in addition to affecting vascular permeability by itself and via activation of procollagenase ($\rightarrow$ metastasis), it facilitates genomic mutation via oxidative cleavage of DNA/RNA or via nitration, oxidation and hydroxylation of guanosine at 8th position, with formation of 8-nitroguanosine and 8-oxoguanosine.[60),62),64)–67)] Furthermore, we found 8-nitroguanosine can be a preferred substrate of cytochrome b_5 reductase (as well as the reductase domain of NOS),[68)] and thus, in the presence of NADPH it can generate superoxide, which reacts with NO generated by NOS, with concomitant formation of $ONOO^-$. $ONOO^-$ then reacts with guanosine, which results in nitration of guanosine and formation of 8-oxoguanosine.[65)–67)] This type of propagation reaction involves a stoichiometry greater than 1:1 (Fig. 5), in that 8-nitroguanosine facilitates formation of both $O_2^{\bullet-}$ and thus $ONOO^-$. The consequence of this process in solid tumor and inflamed tissue is an accelerated production of

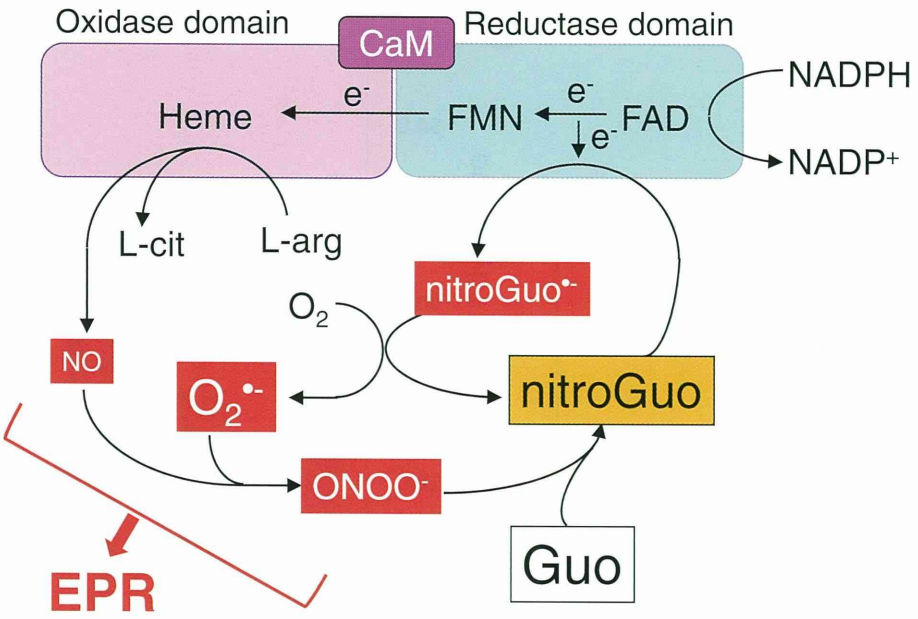

Fig. 5. Scheme of the reaction generating $O_2^{\bullet -}$ via 8-nitroguanosine (nitroGuo) involving nitric oxide synthase (NOS) or cytochrome b_5 reductase in the presence of oxygen and L-arginine.[68] Simultaneous generation of NO and $O_2^{\bullet -}$ results formation of $ONOO^-$, which nitrates guanosine to form 8-nitroGuo; it then becomes substrate of NOS (reductase domain) generating either NO or $O_2^{\bullet -}$, and this reaction continues on. NOS consists of an oxidase domain and a reductase domain. This reductase is similar to cytochrome b_5 reductase that is responsible for $O_2^{\bullet -}$ generation. CaM, calmodulin; FAD, flavin adenine dinucleotide; FMN, flavin mononucleotide; Guo, guanosine; L-cit, L-citrulline.

mutations and thus genetic diversification. Under such circumstances, which generates great genetic diversification, however, it poses a problem against the development of molecular target drug. Recent advances in cancer genomics have provided ample evidence that many human solid cancers undergo disease progression for 10–30 years, and individual malignancies such as breast cancer or colon cancer often have numerous genetic alterations in the same patients.[69)–71)]

Molecular target drug development has aroused great expectations in the cancer treatment community. However, clinical responses to many of these drugs such as antibody drugs are no better than those of conventional anticancer agents.[72),73)] In addition to the very low response rate to these drugs, they are so expensive that the National Institute of Clinical Excellence (NICE) and other agencies in the UK expressed concern about their use,[73)–75)] notwithstanding one rather exceptional success of molecular target drug, imatinib used for chronic myelogenous leukemia.

In this context, tumor targeting via the EPR effect appears to have a more universal application to solid tumors in general, with improved drug delivery, and thus better clinical outcomes (see, *e.g.*, the AT-II-based arterial infusion of SMANCS/Lipiodol section 6.2.1.).

5-3. Prostaglandins, VEGF, carbon monoxide (CO), and cytokines. Prostaglandins and VEGF will result in activation of NOS, and thus generating consequently NO, facilitate the EPR effect, as we described elsewhere.[13),15),16),32)] Other cytokines, including TNF-α, transforming growth factor-β (TGF-β) inhibitor, IL-8, and other inflammatory factors,[76)–78)] may be also involved in the EPR effect involving various mechanisms. Typical examples of cross talk in such factors include bradykinin by inducing cyclooxygenase (COX) II, and eNOS activation[30)–32),34),35)] These cytokines cross talk each other and affect vascular tone.[32),77)]

Very recently, we found that HO-1 (heme oxygenase-1)[79)] is upregulated in many cancers. Consequently the product of HO-1, CO appears to be actively produced during catabolic degradation of heme. This process will facilitate vascular permeability of tumor vessels (Fig. 6A).[79),80)] We also found earlier that suppression of HO-1 leads to tumor regression.[81)–83)] Direct proof of CO as a factor of EPR effect is shown in Fig. 6B.[80)]

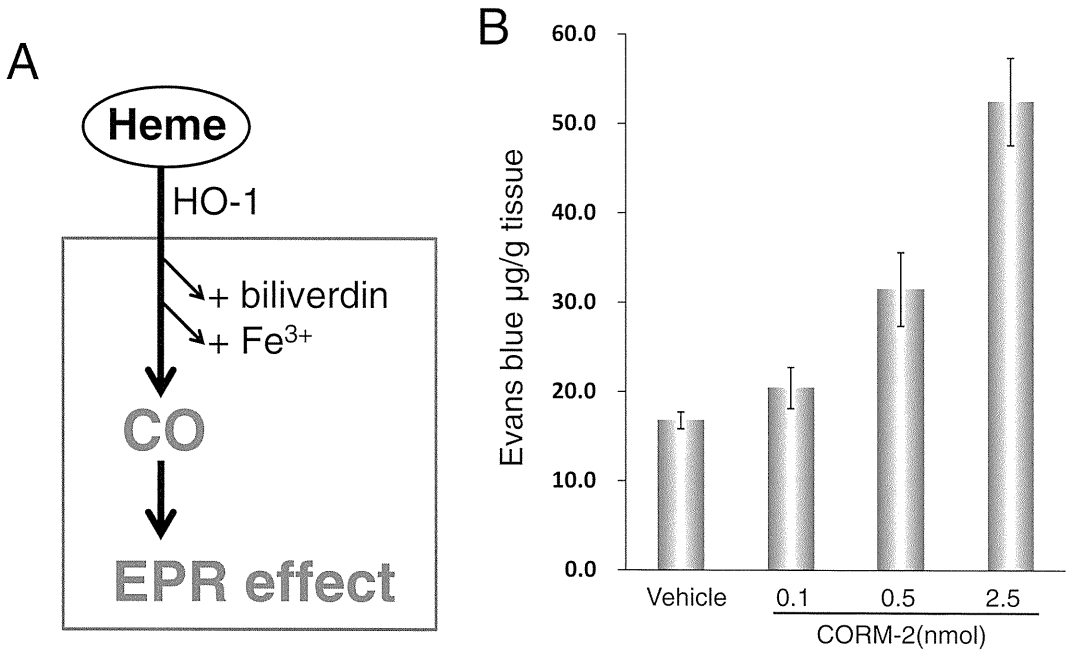

Fig. 6. (A) Hemeoxygenase (HO-1) and enhancement of EPR effect via generation of CO. (A) Role of HO-1 in heme degradation using heme as substrate yields biliverdin, CO, and Fe^{3+}, and CO facilitates the EPR effect. HO-1 is usually up-regulated in most solid cancer cells.[11)–13),63)] (B) CO generating agent CORM-2 (tricarbonyldichlororuthenium dimer) spontaneously decomposes to form CO, thus facilitates EPR effect in a dose dependent manner in mouse skin (ref. 80)) whereas CO trapping agent hemoglobin blocks this.

6. Heterogeneity of the EPR effect and enhancement of tumor-selective drug delivery by augmenting the EPR effect

6-1. Heterogeneity of the EPR effect and drug delivery. In general, solid tumors are quite heterogeneous in terms of histopathology, size, genomics and local environment. For example, a small experimental mouse sarcoma S-180 tumor demonstrates relatively homogeneous EPR effect (*cf.* Fig. 1A); the tumor is completely filled with Evans blue-labeled albumin. The same tumor of large size, however, reveals a large unstained area in the inner core that is either necrotic or hypovascular (Fig. 1B). One could thus argue that the EPR effect is not universal and that it may apply to only a few types of tumor, or small size tumor. In this regard, human HCC (hepatoma) and renal cell carcinoma, which are tumors with high vascular density, show good or homogenous Lipiodol staining when examined by X-ray CT scan in the clinical setting as discussed later. We defined such tumor staining as type A staining.[25),26)] On the contrary to this, the metastatic liver cancer stains predominantly at tumor periphery, defined as type B staining in CT scan image (Fig. 7 A,C,E → B,D,F)[26)] similar to that seen in Fig. 1B. The poor uptake of Lipiodol at the central area in type B staining, however, can be augmented by elevating the systemic blood pressure using angiotensin II (AT-II)-induced hypertension during arterial infusion (Fig. 7 B,D,F). The effect of this AT-II induced hypertension is shown diagrammatically in Fig. 8. Heterogeneity could be also seen in micronodule of metastatic tumor in the liver, as small as 0.5 mm in diameter, which shows a necrotic center of about half the diameter of the micro tumor nodule (Fig. 1C).

The tumor image of Fig. 1B demonstrate that a necrotic center will show no blue albumin leakage near the central area, which is in great contrast to a rapidly growing tumor periphery with blue staining. It is of interest that the growing region of a tumor nodule occurs primarily at the tumor periphery, where it exhibits high EPR effect (*cf.* Fig. 1B) and indeed good macromolecular delivery.[43),84)]

6-2. Modulation of vascular flow and augmentation of drug delivery. In general, metastatic cancers such as metastatic liver cancer are hypovascular as described. Likewise, prostate and pancreatic cancers are tumors with low vascular density. These tumors presumably take up less anticancer agent compared with highly vasculated tumors, and drug

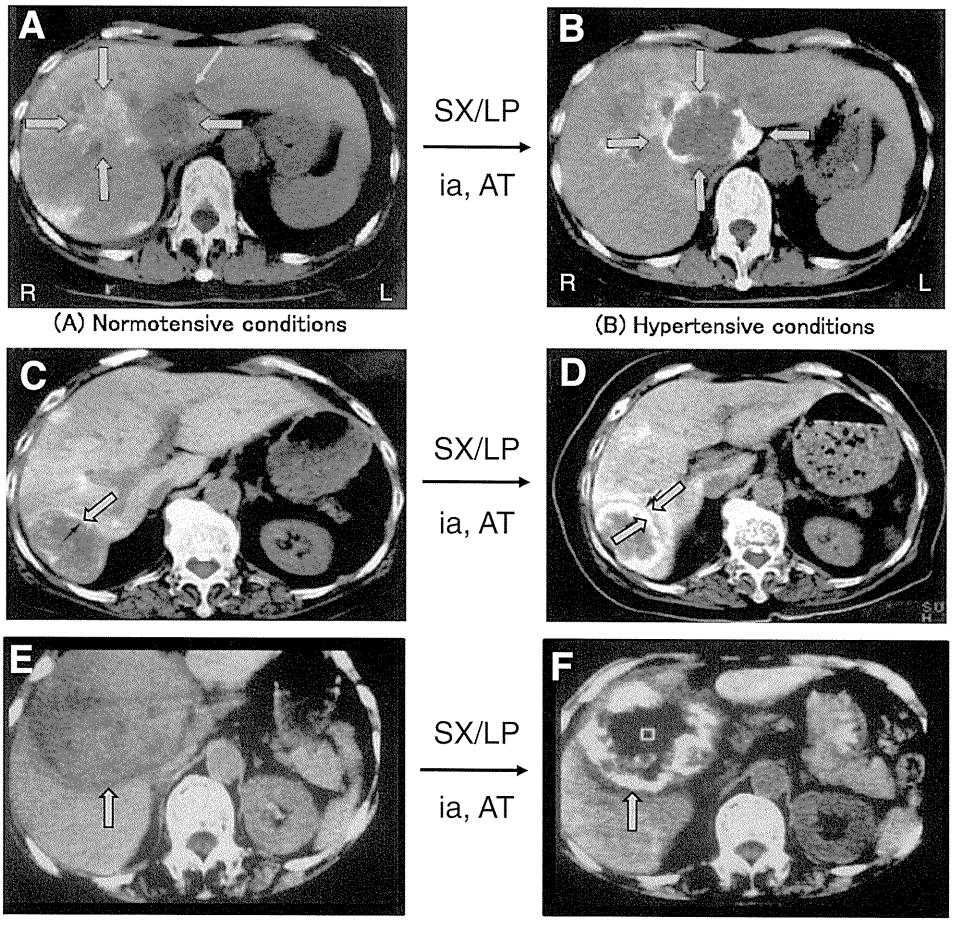

Fig. 7. Retention of SMANCS/Lipiodol in the metastatic liver cancer (A/C/E). (A) and (C) CT scans of images of colon cancers metastasized to the liver. SX/LP (SMANCS/Lipiodol) was infused *via* the hepatic artery under normotension. Retention of drug SX/LP given ia (intraartery) under normotensive state reveal very little drug retention. Three and five days later to (A) and (C), respectively, SX/LP was infused similarly but under AT(angioternsin)-II-induced hypertension; clearly more deposition of the drug near the tumor periphery is clearly seen in (B) and (D). (E) is a massive cholangio cell carcinoma in the liver which did not take-up SX/LP administered ia under normotensive state. Then SX/LP was infused ia under AT-II induced hypertension, and the CT scan reveal intense peripherial staining (F) (*cf.* Fig. 8). All (B), (D) and (F) are classified as type B staining.[26)]

concentrations in such tumors are usually significantly lower than the drug concentrations in plasma. Thus chemotherapy of these tumors is often, if not always, very poor. The hypovascular characteristic and poor blood flow of these tumors with poor drug delivery, can be improved, however, by modulating vascular effectors or by elevating systemic blood pressure via the slow infusion of angiotensin II (AT-II), as well as other means as described below.

6-2-1. Augmentation of the EPR effect by modulating tumor blood flow by raising blood pressure. As demonstrated by Suzuki *et al.*[85)] and Hori *et al.*[86)] of Tohoku University, blood flow in tumor tissues can be increased by raising the systemic blood pressure; for instance, from 100 mmHg (normal) to 150 mmHg by slow intravenous infusion of AT-II. The blood flow volume (rate) in normal tissue, in contrast, remains constant regardless of artificially elevated blood pressure. Under this AT-II-induced hypertension, a relatively hypovascular tumor image can be changed to well vascularated image with rich blood flow[86)] as seen in angiogram being highly stained (Fig. 9A vs. 9B). The same angiographic enhancement will be seen in the clinical setting. For example, a metastatic abdominal tumor, originating from liver cancer was visualized in abdominal cavity clearly (Fig. 9C vs. 9D, see circled area at right), only by using AT-II induced hypertension. This hypertension facilitates tumor selective drug delivery and contrast agent (*cf.* Figs. 8–11), while reducing leakage of drug from

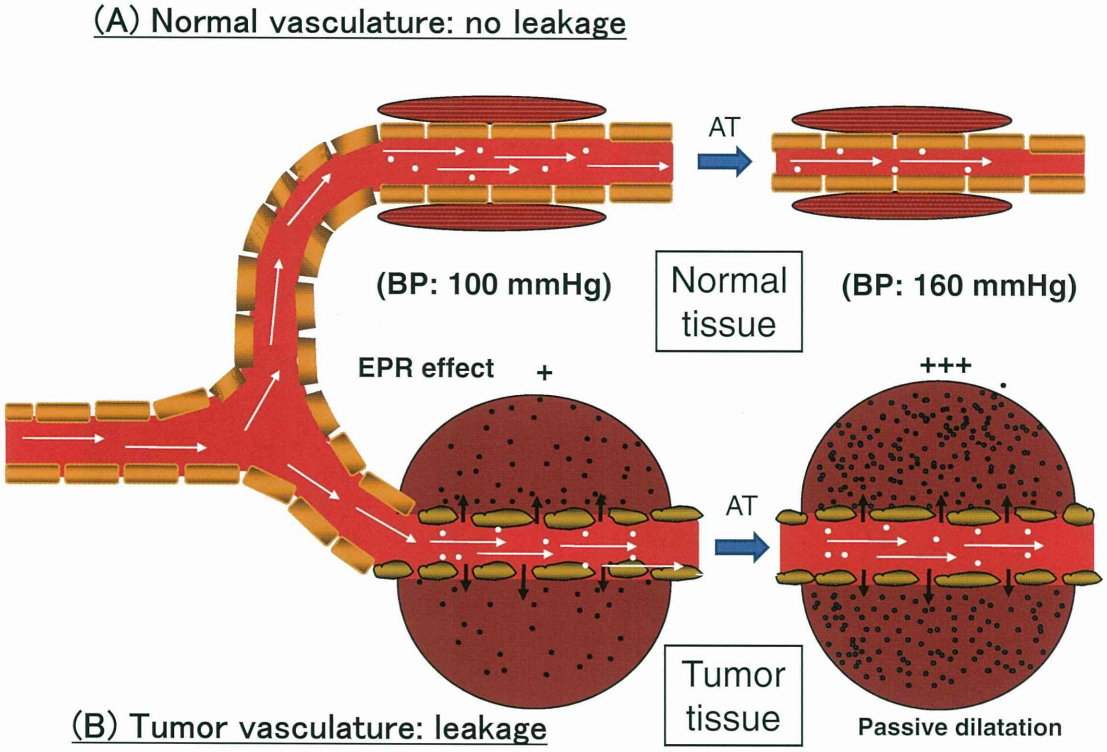

Fig. 8. Diagrammatic representation of EPR effect and effect of angiotensin(AT)-II-induced enhancement of the EPR effect and drug delivery in tumor tissue (lower half). Please compare the situation in normal tissue in the upper half. AT-II infusion induced high blood pressure (BP) (*e.g.*, 100 → 160 mmHg) that caused endothelial cell-cell junctions to open hydrodynamically only in tumor vasculature (lower right). The normal blood vessels (upper right), in contrast, have surrounding smooth muscle-cell layer that will contract and tighten the cell-cell junctions, and a narrowing of the vascular diameter will cause less leakage of drugs. AT-II induced hypertension thus result in more delivery of macromolecular drugs to tumor (See lower right) (Adapted from Maeda[36] with modification).

blood vasculature in normal tissue, thus preventing adverse side effects.[87),88)] The arterial infusion of SMANCS/Lipiodol under AT-II-induced hypertension markedly enhanced the delivery (Fig. 7 A,C,E → B,D,F/Fig. 10 C,E → D,F/Fig. 11 A,C → B,D) and therapeutic effect was much improved (Figs. 10,11).[30)–32),88)]

The most remarkable therapeutic consequences of AT-II-induced hypertension were observed in patients with difficult-to-treat advanced cancers—metastatic liver cancer, cancers of the gallbladder, bile duct, pancreas, and kidney, and primary liver cancers[88)] (Figs. 10,11). Beneficial effects included a shorter time to achieve tumor regression. In the normotensive state, massive HCCs (diameters >5 cm) needed three arterial infusions in 6 months to reduce the tumor volume to 10% of the original size. With AT-II-induced hypertension, however, only one infusion produced a remarkable response in one month.[88)] Many metastatic liver cancers regressed to less than 10% of the original tumor volume in 1–2 months without appreciable toxicity such as bone marrow suppression, or damage to the kidney or the liver.[88)]

6-2-2. Augmentation of the EPR effect by utilizing NO-releasing agents. As described above, we found that NO plays an important role in the vascular permeability and growth of solid tumors.[11)–13),35)] During my research, I conceived an analogy between hypoxic solid tumor (hence showing less staining) and infarcted cardiac tissue (as in angina pectoris), because both are similarly hypoxic.[89),90)] In the latter case use of nitroglycerin (NG) has been recognized for more than a century. NG liberates nitrite by action of denitrase, and nitrite is then converted by nitrite reductase to NO in the infarcted tissue.[91)–93)] This pharmacological benefit of NG was also validated in mouse tumor models *in vivo* that showed an improved therapeutic effect when anticancer agents were combined with NG.[35),89)] Figure 12A illustrates the mechanism of NO generation in solid tumor. An application of NG ointment to the skin of tumor-

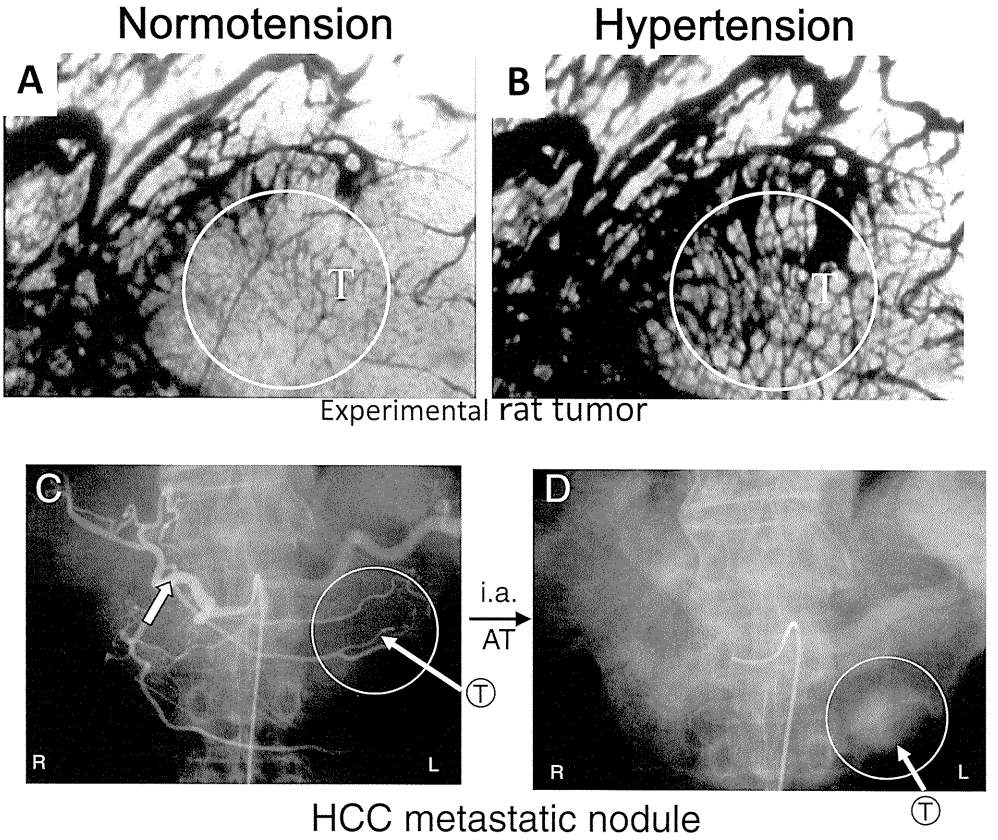

Fig. 9. Visualization of hypovascular tumor by AT-II-induced hypertension. (A) Under normal blood pressure, this tumor, encircle mark T, in which rat Yoshida LY80 tumor was clamped with Lucite® window, shows only weak blood flow. (B) Blood flow became highly visible under AT-II-induced hypertension (adapted from Hori *et al.*[86]). This type of enhanced angiographic staining can be observed with human case. As seen in the angiogram (C), (D), which show an abdominal metastatic tumor (encircled T) from the primarily liver cancer; it is only visible after AT-II-induced hypertension (D). Under the normotensive state of arterial phase angiography, no tumor was revealed in the circle area at the lower left (C). But AT-II-induced angiography at the venous phase demonstrated easily detectable tumor in (D) (arrows in circled area at the lower right) (C and D adapted from ref. 36)).

bearing mice produced increased blood flow in only tumor tissue, but not in normal tissue, and hence increased macromolecular drug delivery to tumor was achieved (Fig. 12 B,C).

Clinical evaluations of NG used in combination with conventional low MW anticancer agents were recently undertaken by Yasuda *et al.*[94)–96)] and Siemens *et al.*[97)] and both studies showed significant clinical improvement in therapeutic response. In earlier study NG was found to enhance the therapeutic effect of radio therapy of cancer.[98)] By the administration of NG, enhanced blood flow resulted higher pO_2 of tumor tissue, consequently better therapeutic outcome.[93),98)] Higher pO_2 of cancer tissue also facilitated the modulation of cellular signaling such as HIF-1α (hypoxia inducible factor) that down-regulation of growth signals (VEGF) or their further signaling pathway.[94),96)] These data therefore indicate that NO clearly benefits patients undergoing chemotherapy. Also, nitro agents per se showed tumor suppression in animal models and in humans.[89),95)]

6-2-3. Augmentation of EPR effect by using ACE inhibitors and a prostaglandin I_2 agonist (beraprost sodium). Another line of research on enhancing tumor drug delivery concerns the use of angiotensin converting enzyme (ACE) inhibitors. ACE can degrade angiotensin-I (AT-I) to generate AT-II, which results in hypertension. On the other hand, ACE also inhibits degradation of (brady)kinin, whose C-terminal amino acid sequence is similar to that of AT-I. Consequently, it results in an increased local concentration of kinin, and hence vascular permeability of tumor will be increased, as will delivery of drugs, including the antibody IgG.[31),35),99),100)] ACE inhibitors are nontoxic, usually producing no adverse